(28) Sakai, H.; Tomiyama, K.; Sou, K.; Takeoka, S.; Tsuchida, E. *Bioconjugate Chem.* **2000**, *11*, 425–432.
(29) Sakai, H.; Yuasa, M.; Onuma, H.; Takeoka, S.; Tsuchida, E. *Bioconjugate Chem.* **2000**, *11*, 56–64.
(30) Vandegriff, K. D.; McCarthy, M.; Rohlfs, R. J.; Winslow, R. M. *Biophys. Chem.* **1997**, *69*, 23–30.
(31) Armstrong, J. K.; Wenby, R. B.; Meiselman, H. J.; Fisher, T. C. *Biophys. J.* **2004**, *87*, 4259–4270.
(32) *Kobunshi-Kagakuno Kiso (Basics of Polymer Science)*; Japanese Society of Polymer Science, Ed.; Tokyo Kagaku Dojin Publisher: Tokyo, Japan, 1978.
(33) Asakura, S.; Oosawa, F. *J. Polym. Sci.* **1958**, *33*, 183–192.
(34) Otsubo, Y. *Langmuir* **1995**, *11*, 1893–1898.
(35) Otsubo, Y. *Heterogeneous Chem. Rev.* **1996**, *3*, 327–349.
(36) Sou, K.; Endo, T.; Takeoka, S.; Tsuchida, E. *Bioconjugate Chem.* **2000**, *11*, 372–379.
(37) Makino, C.; Kimura, N.; Hasegawa, E.; Tsuchida, E. *Nippon Kagaku Kaishi* **1991**, *8*, 1102–1105.
(38) Kawakami, K.; Nishihara, Y.; Hirano, K. *J. Phys. Chem. B* **2001**, *105*, 2374–2385.
(39) Oosawa, F.; Asakura, S. *J. Chem. Phys.* **1954**, *22*, 1255–1256.
(40) Vincent, B.; Luckham, P. F.; Waite, F. A. *J. Colloid Interface Sci.* **1980**, *73*, 508–521.
(41) Neu, B.; Meiselman, H. J. *Biochim. Biophys. Acta* **2006**, *1760*, 1772–1779.
(42) Vincent, B.; Edwards, J.; Emmett, S.; Jones, A. *Colloids Surf.* **1986**, *18*, 261–281.
(43) Donath, E.; Krabi, A.; Allan, G.; Vincent, B. *Langmuir* **1996**, *12*, 3425–3430.
(44) Sou, K.; Tsuchida, E. *Biochim. Biophys. Acta* **2008**, *1778*, 1035–1041.
(45) Chen, R. Y.; Carlin, R. D.; Simchon, S.; Jan, K. M.; Chien, S. *Am. J. Physiol. Heart Circ. Physiol.* **1989**, *256*, H898−H905.
(46) Tsai, A. G.; Intaglietta, M. *Biorheology* **2001**, *38*, 229–237.
(47) Tsai, A. G.; Acero, C.; Nance, P. R.; Cabrales, P.; Frangos, J. A.; Buerk, D. G.; Intaglietta, M. *Am. J. Physiol. Heart Circ. Physiol.* **2005**, *288*, H1730−H1739.
(48) de Wit, C.; Schafer, C.; von Bismarck, P.; Bolz, S. S.; Pohl, U. *Pflugers Arch.* **1997**, *434*, 354–361.
(49) Contaldo, C.; Schramm, S.; Wettstein, R.; Sakai, H.; Takeoka, S.; Tsuchida, E.; Leunig, M.; Banic, A.; Erni, D. *Am. J. Physiol. Heart Circ. Physiol.* **2003**, *285*, H1140−1147.
(50) Plock, J. A.; Contaldo, C.; Sakai, H.; Tsuchida, E.; Leunig, M.; Banic, A.; Menger, M. D.; Erni, D. *Am. J. Physiol. Heart Circ. Physiol.* **2005**, *289*, H2624−H2631.

BM900455E

総　説

ヒト血清アルブミンを用いた機能分子・材料の創製

Synthesis of Functional Molecules and Materials Based on Human Serum Albumin

小松 晃之[1, 2]，屈　雪[1]，土田 英俊[1]，中川 晶人[1]

Teruyuki Komatsu [1, 2], Xue Qu [1], Eishun Tsuchida [1], Akito Nakagawa [1]

和文抄録

筆者らはヒト血清アルブミン（HSA）の多分子結合能を利用して，その内部に機能性分子を包接させる方法や，さらにはHSAと高分子電解質の交互積層膜を多孔性膜の細孔内で作成する方法により，自然界には見ることのできないユニークな機能分子・材料を創製してきている．HSAに鉄テトラフェニルポルフィリン誘導体（FeP）を包接させたHSA-FeP複合体は生理条件下で酸素を可逆的に結合解離できる人工酸素運搬体となり，遺伝子組換えアルブミン（rHSA）にヘモグロビンの活性中心である鉄プロトポルフィリン（heme）を結合させたrHSA-heme錯体も酸素吸脱着のできる人工ヘム蛋白質となる．一方，HSA－亜鉛プロトポルフィリン錯体は水の光還元による水素発生反応の増感剤として作用し，HSA－カルボキシフラーレン複合体は一重項酸素生成の光増感剤として腫瘍光線力学療法への応用が期待されている．さらに，多孔性ポリカーボネート膜をテンプレートとした鋳型内交互積層法により，HSAからなる中空シリンダー構造のナノチューブが合成できる．これらの新機能分子・材料の特徴と応用展開について，最近の話題を紹介する．

Abstract

We have synthesized unique functional molecules and materials based on human serum albumin (HSA), which have never seen in nature, by means of incorporation of functional ligands into the protein or fabrication of layer-by-layer assembly in the nanoporous membrane. HSA incorporating iron (II) tetraphenylporphyrin derivative (FeP) (HSA-FeP) is an artificial O_2 carrier which can reversibly binds and release O_2 under physiological conditions. Recombinant HSA complexed with a natural iron (II) protoporphyrin IX (heme) (rHSA-heme) also acts as O_2 transport hemoprotein. On the other hand, HSA complexed with a zinc (II) protoporphyrin IX functions as a photosensitizer for H_2 evolution from water, and HSA-carboxy fullerene hybrid produces singlet O_2 by visible light irradiation; it may be used as a sensitizer in photodynamic cancer therapy. Furthermore, HSA nanotubes are prepared by layer-by-layer deposition technique using porous polycarbonate membrane template. We highlight recent development and applications of these functional molecules and materials.

Keywords

Human serum albumin, albumin-heme, oxygen carrier, red blood cell substitute, photosensitizer, nanotubes

1．はじめに

ヒト血清アルブミン（HSA）は血清蛋白質の約60％を占める補欠分子族を持たない単純蛋白質（分子量：66,500）であり，血流中ではコロイド浸透圧維持のほか，各種内因性・外因性物質（脂肪酸，ヘミン，ビリルビン，金属イオン，ホルモン，NO，薬物）の運搬・貯蔵，pH緩衝作用，エステラーゼ活性などの役割を担っている[1-3]．1992年，米国国立航空宇宙局（NASA）のCarterらはHSAの高分解能X線結晶構造解析（分解能：2.8 Å）に成功し，その三次元構造の全容を明らかにした[4]．585個のアミノ酸からなる一本鎖ポリペプチドは17個のジスルフィド結合を介してハート形に折りたたまれ（長径：約8 nm，厚み：約3 nm），相同性の高い3つのドメインI～III

(1) 早稲田大学 理工学術院 総合研究所（理工学研究所） 〒169-8555 東京都新宿区大久保3-4-1 Research Institute for Science and Engineering, Waseda University, 3-4-1 Okubo, Shinjuku-ku, Tokyo 169-8555, Japan

(2) 科学技術振興機構さきがけ 〒332-0012 埼玉県川口市本町4-1-8 PRESTO, Japan Science and Technology Agency (JST), 4-1-8 Honcho, Kawaguchi-shi, Saitama 332-0012, Japan

論文受付 2009年5月7日　論文受理 2009年5月22日

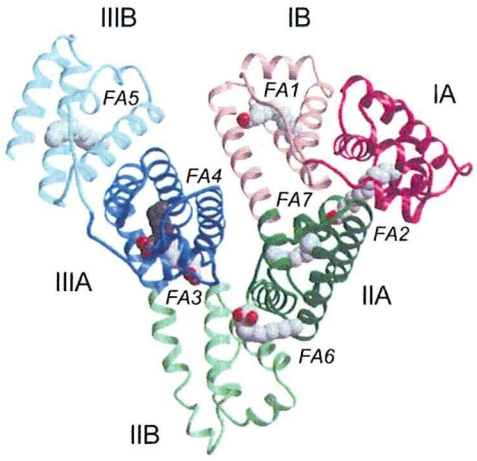

Fig. 1. Structure of HSA with seven myristic acids (PDB 1e7g). The protein secondary structure is shown schematically and the domains are colored (I; red, II; green, III; blue). The A and B subdomains are depicted in dark and light shades. respectively. The fatty acid binding sites are represented from FA1 to FA7 in italics.

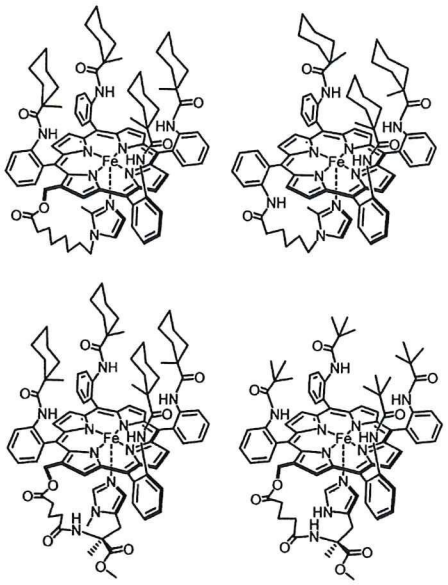

Fig. 2. Chemical formula of typical FeP molecules that can be incorporated into HSA to form HSA-FeP hybrid.

を構成している（各ドメインはさらに２つのサブドメインA，Bに分けられる．Fig. 1）．Sudlowらが提唱した古典的なHSAの薬物結合サイトI（ワルファリン，インドメタシンなど）はサブドメインIIA，薬物結合サイトII（ジアゼパム，イブプロフェンなど）はサブドメインIIIAに相当する[5]．

一方，HSAは遺伝子組換え技術により大量発現が可能な蛋白質である[6]．近年，その多分子結合能と高い生産性に注目が集まり，HSAに金属錯体を包接させた人工蛋白質の構築が盛んになってきている．例えば，GrossらはHSAにマンガンコロールを結合させた複合体を調製し，スルフィドの立体選択的酸化触媒として利用した[7]．また，ReetzらはHSAに銅フタロシアニンを結合させた複合体が，Diels-Alder反応に有用であることを明らかにした[8]．

本稿では，酸素運搬体，光増感剤から，蛋白質ナノチューブまで，著者らが進めているHSAを利用した新しい機能分子・材料の創製と応用について最近の話題を紹介したい．

2．アルブミン－脂肪酸複合体の結晶構造解析

HSAの最もよく知られたリガンドに脂肪酸がある．1998年，CurryらはHSA－脂肪酸複合体のX線結晶構造解析に初めて成功し，中・長鎖脂肪酸の結合サイト（FAサイト）を特定した[9,10]．HSAには全ての脂肪酸に共通する７個のサイトがあり（Fig. 1），FAサイト１，４，５，７は各サブドメインの中央に，FAサイト２，３は二つのドメインの境界面に，そしてFAサイト６は二つのサブドメインの境界面に位置する．FAサイト１－５では，脂肪酸の末端カルボキシル基が塩基性または極性アミノ酸残基と相互作用することによりしっかりと固定されている．これら５つのうちどこが最も親和性の強い部位なのか，結晶構造からは判定できない．組換えHSAの詳細な^{13}C-NMRスペクトル測定から，FAサイト２，４，５が親和力の強いサイトであることが明らかにされた[11]．７つのFAサイト全てに脂肪酸が結合すると，HSA全体の分子形態はダイナミックに変化する．特にドメイン間に存在するFAサイト２，３への結合は，ドメインIIを軸として大きな形態変化を誘起した．HSAの二次構造はα-ヘリックスが67％，β構造が０％である．古くから脂肪酸などのリガンド結合によりHSAの二次構造が変化するという報告があるが，リガンド結合後も二次構造に変化はないことが結晶学的に示された．Curryらはその後も各種HSA－リガンド複合体の結晶構造解析を系統的に進め，多くの複合体について構造を解明している[12-14]．現在Protein Data Bank（PDB）に登録済みのHSA－リガンド複合体のデータ47件のうち，37件はCurryらによるものである．

3．アルブミン－合成ヘム複合体（人工酸素運搬体）

我々は独自の分子設計により合成した鉄テトラフェニルポルフィリン誘導体（合成ヘム：FeP）をHSAに包接させたアルブミン－ヘム（HSA-FeP）複合体が，生理条件下でヘモグロビン（Hb）と同じように酸素を吸脱着できることを見出した[15-18]．これまでに約30種類以上のFeP（Fig. 2）を合成し，その酸素結合能とヘム構造の相関を整理してきている[19-22]．酸素錯体の安定度は天然のミオグロビン（Mb）を上回り，酸素親和性（P_{50}）は0.1 Torrから230 Torrまで所望の値に揃えることができる．つまり，適用に応じた製剤の選択が可能となっている．HSA-FeP溶液の血液適合性は高く，血液凝固系，補体系，血小板の活性化に対しても影響を及ぼさない[23]．室温で２年以上の棚置保存が可能で，その間酸素結合パラメーターに変

化はない[24]．脱血交換試験（ラット，ビーグル犬）から出血ショック状態からの蘇生効果，生体内における酸素輸送能が証明されている[25,26]．体内投与後も修飾Hb製剤に見られるような血管内皮細胞からの漏出，一酸化窒素捕捉に伴う血管収縮，血圧亢進は全く観測されない[27]．これはHSAの表面電荷が負に帯電しているため血管から漏れ出しにくいことに起因すると考えられており，本製剤の最大の利点となっている．

一般に悪性腫瘍は放射線療法や化学療法に抵抗性を示し，その原因の一つとして腫瘍組織内低酸素細胞（hypoxic cell）の存在があげられる．細胞の異常な増殖により新生血管の生成が追いつかない湿潤性腫瘍細胞では，十分な血流および酸素化が得られず，それが治療の妨げとなっている．HSA-FeP溶液を腫瘍組織の患部近傍へ投与し，腫瘍組織内低酸素細胞の酸素化を試みたところ，患部の酸素分圧は投与前の2.5倍に増大した[28]．これは，従来報告されている修飾Hb製剤を用いた処置に比べて格段に高く[29]，粒子径の小さいHSA-FePが腫瘍内部へ容易に到達できるためと考えられる．実際に放射線療法と併用した結果，HSA-FeP投与による抗癌作用の顕著な増強効果が認められた[30]．また，HSA-FePの分子表面をポリ（エチレングリコール）で被覆すると，血中滞留時間が大幅に延長されることも明らかにされている[31,32]．

4．遺伝子組換えアルブミンープロトヘム錯体（人工酸素運搬体）

アルブミン一合成ヘム複合体の酸素結合部位は，精密に分子設計された鉄テトラフェニルポルフィリン誘導体（FeP）であり，得られたHSA-FeP複合体が酸素を可逆的に結合解離できることは，錯体化学的に見れば設計通りの機能発現といえる．HSAを用いた人工酸素運搬体開発における究極の挑戦は，やはりHbの酸素結合部位であるヘム鉄［鉄プロトポルフィリンIX（プロトヘム，heme)］(Fig. 3a）を用いた製剤の確立であろう．2004年，我々は遺伝子組換え技術を用いてアミノ酸の一部を改変した組換えHSA（rHSA）にhemeを包接させたrHSA-heme錯体が，水中で酸素を吸脱着できることを見出した[33]．

溶血により血中に放出されたメトHbから解離した鉄（III）プロトポルフィリンIX（hemin）は，通常ヘモペキシンと呼ばれる糖蛋白質に捕捉されるが[34]，ヘモペキシンの血中濃度は約17μMと低いため，遊離heminの多くは一旦HSAに結合し肝臓へと運ばれる．HeminがHSAに捕捉されることは昔から知られていた．1938年，Fairelyはheminと相互作用する血清蛋白質がHSAであることを発見し，その複合体をhemalbuminと名付けた[35]．それ以来，このHSA-hemin錯体は，何らかの生理作用があるのではないかと研究者達の関心の的となってきた．1975年，Muller-Eberhardらにより HSA-hemin錯体の吸収スペクトルが報告され，heminの中心鉄にアミノ酸残基が軸配位した高スピンヘム錯体構造が推定された[36]．また，1980年にはBermanらがHSAとheminの結合定数（K：$1.1\times10^{8}\ M^{-1}$）を決定[37]，この値は脂肪酸に比べて約100倍高く，heminがHSAに強く結合することが明確となった．

2002年，Carterと我々のグループは独立にHSA-hemin錯体のX線結晶構造解析に成功し，heminがHSAのサブドメインIB内の疎水ポケットに結合していることを明らかにした[38,39]．この部位は，脂肪酸のFAサイト1に相当する．heminの中心鉄にはチロシン（Tyr)-161のフェノレート酸素が軸配位し，二つのプロピオン酸残基は，三つの塩基性アミノ酸残基（リシン，ヒスチジン，アルギニン）と相互作用していることがわかった（Fig. 3b)．よく知られているようにMbのヘムポケット内では，ヘム中心鉄にヒスチジン（His)-93が軸配位し，そのトランス側（第6配位座）に酸素分子が結合する（Fig. 3c)．さらに，配位酸素側にはもう一つのHis-64が遠位塩基として存在し，酸素錯体を安定化している．ここで両者を見比べてみると，誰もがその構造類似性に気づくであろう．しかし，残念ながらHSA-hemin錯体の中心鉄を鉄（Ⅱ）に還元して酸素を吹き込んでみても，酸素錯体は得られない[33]．それは軸配位子がHisではないためである．HSA-hemin錯体が血中で何らかの役割をはたしているのではないかという期待とは裏腹に，むしろHSAはhemin分子の活性を巧みに抑え込んでいたのである．しかしながら，hemeが疎水的な分子空間に配置された構造はMbのヘムポケットと共通しているので，それならばHSAの場合でもヘム鉄の配位圏内（サブドメインIB）にHisが存在すれば，酸素錯体ができるのではないかと考えた．そこで遺伝子組

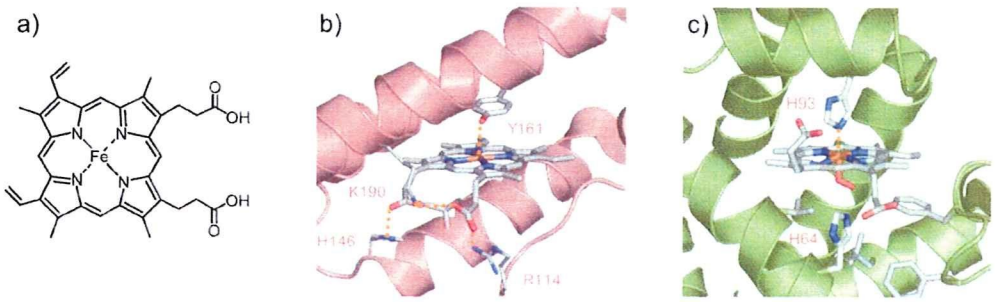

Fig. 3. (a) Chemical formula of iron (II) protoporphyrin IX (heme). Heme pocket structures of (b) HSA-hemin complex (PDB 1o9x) and (c) oxy-Mb (pdb 1mbo).

換え技術を用いて，イソロイシン（Ile）-142位置へ近位塩基として働くHisを変異導入し，さらに中心鉄に軸配位しているTyr-161を疎水性アミノ酸（ロイシン（Leu））に変換したところ，その組換えHSA-heme［rHSA（I142H/Y161L）-heme］錯体は，室温で酸素を吸脱着することができた[33,40]．rHSAとhemeから構成される酸素輸送人工ヘム蛋白質の初めての例である．そこで，酸素結合パラメーターを詳細に解析した．rHSA（I142H/Y161L）-heme錯体の$P_{1/2}$は18 Torr（22℃）であり，Hb，Mb，ヒト赤血球の値に比べて高い（酸素親和性は低い）．rHSA（I142H/Y161L）-heme錯体の低い酸素親和性は，速度論的には大きな解離速度定数（k_{off}）に起因した[33,40]．rHSAの中ではhemeを取り巻く分子環境が疎水的であるためにk_{off}が高く，酸素親和性が低く抑えられているのである．

このように酸素錯体は得られたものの，実際にrHSA（I142H/Y161L）-heme錯体を人工酸素運搬体として利用するためには，その酸素親和性をHbや赤血球の値に近づけなければならない．そこで，第三の変異を導入することにより，酸素親和性を上げる工夫を行った．前述したように，HbやMbのヘムポケット内には酸素配位座側にHis-64が遠位塩基として存在し，酸素親和性の増大に寄与している[41,42]．我々はrHSAの場合も，酸素配位座側の適当な位置に遠位塩基を導入すれば，酸素親和性が上昇するのではないかと考えた．分子シミュレーションの結果から配位酸素直上のLeu-185を選定し，そこへ遠位塩基としてのアスパラギン（Asn）を導入した［rHSA（I142H/Y161L/L185N）］[43]．rHSA（I142H/Y161L/L185N）-heme錯体（Fig. 4）の可視吸収スペクトルは，窒素雰囲気下では鉄（II）5配位高スピン錯体の形成を示し，そこへ酸素を通気すると速やかに酸素錯体型へと移行した．$P_{1/2}$は1 Torr（22℃）となり，酸素親和性はもとの二重変異体に比べて18倍も上昇した．Asnの導入によりヘムポケットの極性が増大しk_{off}が減少した結果，酸素親和性が上がったものと考えられる．rHSA（I142H/Y161L/L185N）-heme錯体は，Hbと同等の酸素親和性を有する人工ヘム蛋白質となった．つまり我々は，本来補欠分子族すらもたない単純蛋白質のHSAに，酸素結合能を付与することに成功したばかりでなく，ヘムポケットの微小空間を部位特異的アミノ酸置換により最適化することで，酸素親和性のコントロールを実現したのである．

ごく最近，酸素配位座側にあるアルギニン（Arg）-186を疎水性アミノ酸に変換すると，酸素親和性がヒト赤血球と同等値に調整できることを見出した[43]．rHSA-heme錯体は天然のプロトヘムを活性中心とする，いわば“酸素輸送のできる赤色の血清蛋白質”である．臨床利用可能な赤血球代替物として，現在実用化に向けた努力が進められている．

5．アルブミン－亜鉛プロトポルフィリン錯体（水素発生の光増感剤）

ポルフィリン化合物の最大の魅力は，その中心金属を変えることにより多彩な機能を発揮できる点にある．特に可視光領域に大きな吸収帯を持つ特徴を生かして，光反応の増感剤として広く利用されている．しかし，鉄ポルフィリン錯体は光励起状態の寿命がきわめて短いため，一般的には光反応の増感剤には適さず，励起寿命の長い亜鉛錯体が用いられる．

水素（H_2）は二酸化炭素排出のない近未来のクリーンエネルギーである．Grätzelらは亜鉛テトラメチルピリジニウムポルフィリンをメチルビオロゲン（MV^{2+}）／白金コロイド／EDTA水溶液に加え可視光照射すると，水の光還元反応が進行し水素が得られることを見出した[44]．もしプロトポルフィリンIX（PP）が水の光還元に利用できれば，天然物質を増感剤とした水素発生システムが確立できることになる．しかし，亜鉛プロトポルフィリンIX（ZnPP）は水に不溶で，そのまま使用することは難しい．そこで，ZnPPをHSAに包接させることによりHSA-ZnPP錯体とし，水の光還元反応への応用を試みた．HSA-ZnP錯体水溶液にMV^{2+}を加え，アルゴン雰囲気下でレーザーフラッシュ（532 nm）を照射すると，ZnPの励起三重項状態からMV^{2+}への電子移動反応が観測された[45]．続いて，白金コロイド，犠牲試薬としてのトリエタノールアミンを加え可視光照射してみると，速やかに水の還元が起こり溶液中から水素が発生した（Fig. 5）．水素発生効率は亜鉛テトラメチルピリジニウムポルフィリンを用いた場合よりも高い．つまり，HSA-ZnPP錯体は水の光還元反応における有効な増感剤として機能する．

この結果は，アルブミン－ポルフィリン錯体においてポルフィリンの中心金属を変えることにより，様々な機能を持った人工蛋白質が創製できることを示唆している．

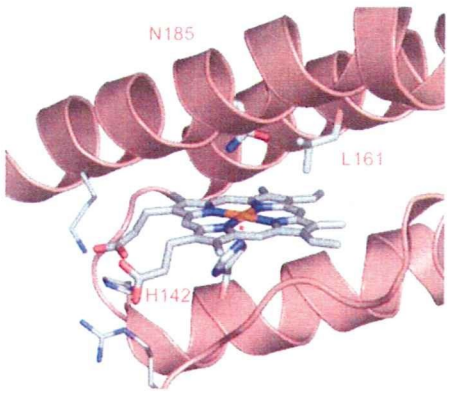

Fig. 4. Structural model of the heme pocket in rHSA (I142H/Y161L/L185N)-heme complex.

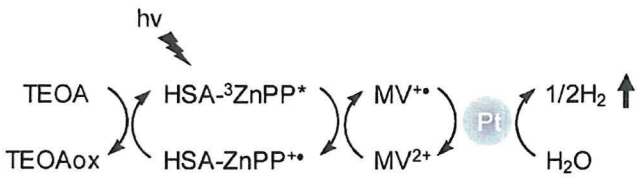

Fig. 5. Reaction scheme of photoreduction of water to hydrogen using HSA-ZnP complex.

6．アルブミン－フラーレン複合体（光線力学療法の増感剤）

金属ポルフィリン以外の機能性分子でもHSAに包接させれば，新しい人工蛋白質が合成できるはずである．そこで，HSAにフラーレン誘導体を包接させたアルブミン－フラーレン複合体を調製し，その構造，光物性，光線力学療法（photodynamic therapy: PDT）における増感剤としての可能性について検討した．現在，よく知られているPDTの光増感剤には，ヘマトポルフィリンの誘導体であるフォトフリン[46,47]，プロトポルフィリンの前駆体である5-アミノレブリン酸[48]，またクロリン誘導体であるビスダイン[49]などがある．これらのポルフィリン誘導体に比べ，フラーレンC_{60}は高い光安定性を持ち，一重項酸素生成の量子収率が高いことから，PDTの新しい増感剤として期待されている[50-52]．

HSAにカルボキシフラーレン（CF，Fig. 6a）を包接させたHSA-CF複合体はきわめて安定で，その水溶液は調製2年後でも沈殿・凝集など全く認められなかった（Fig. 6b）[53]．可視吸収スペクトル，HPLC，質量分析の結果から，HSAとCFが1：1で結合していること，さらに小角X線散乱測定から，CF結合後もHSAの分子径，表面電荷に変化はないことがわかった[53]．

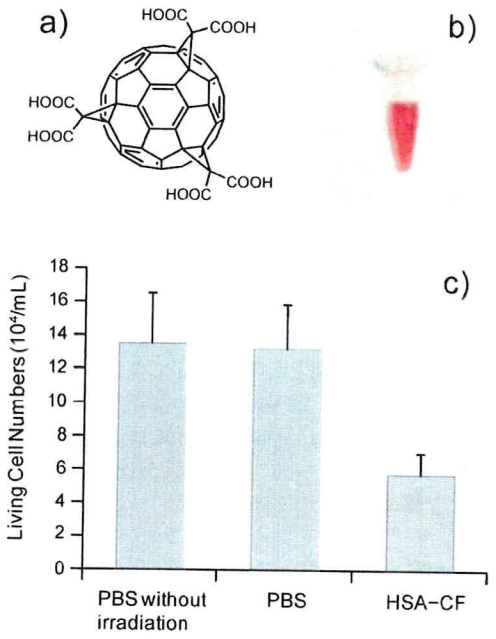

Fig. 6. (a) Chemical formula of carboxy-C_{60}-fullerene, (b) red colored solution of aqueous HSA-CF, and (c) living cell numbers of LY80 with HSA-CF and PBS after visible light irradiation (20 mW cm^{-2}, 2 h, 36±1℃). Each value represents the mean ± SD (n = 4).

一般に色素分子を光励起すると，まず励起一重項状態を形成し，そこから項間交差により励起三重項状態へと遷移する．一重項酸素生成の有効な光増感剤となるためには，この励起三重項状態が安定でなければならない．HSA-CF複合体の励起三重項寿命は46 μsと長く，それはCFが蛋白質内部に固定されているため，励起種どうしによる消光が抑えられることによる．系内に酸素を共存させると，励起三重項状態から酸素分子へのエネルギー移動が観測された．生成する一重項酸素は1270 nmに蛍光を示すので，その強度から一重項酸素生成の量子収率が算出できる．HSA-CF複合体の量子収率は0.46であり，HSA-PP複合体やメチレンブルーと同程度であったことから[54]，本化合物が一重項酸素生成の有効な光増感剤として作用することがわかった．

続いてこの製剤の細胞毒性について検証した．腫瘍細胞（LY80）にHSA-CF水溶液を加え，まず暗所下でそれ自身に細胞毒性がないことを確認．その後ハロゲンランプを用いて光照射（2 hr）すると，細胞数は43％にまで減少した（Fig. 6c）[53]．この結果はHSA-CF複合体がPDTの光増感剤として有効であることを示している．

7．アルブミンナノチューブ（分子捕捉剤，薬物運搬体，ナノリアクター）

ピキア酵母を用いた遺伝子組み換え体の量産体制が確立して以来，HSAは臨床利用はもちろんバイオマテリアルの有用な素材としても注目を集めている[6]．我々は最近，鋳型内交互積層法によりHSAからなる中空シリンダー構造のナノチューブを合成することに成功した[55-57]．HSAの等電点は4.8と低く，生理条件下では分子表面が負に帯電している．上述したようにHSAがHbに比べて血管外へ逸脱し難いのは，血管内皮細胞の外側にある基底膜との静電反発による．そこでまず正電荷を有する高分子電解質（例えば，ポリ-L-アルギニン（PLA）などのポリアミノ酸やポリエチレンイミンなど）を多孔性ポリカーボネート（PC）膜の細孔内に通過させ，続いてHSA水溶液を通過させる．この操作を繰り返しながら，細孔内壁にHSAの多重積層膜を作成し，最後にPC膜を溶解除去すると，HSAからなる均一で柔軟なナノチューブが得られる．孔径400 nmのPC膜にPLAとHSAを各3回ずつ通過させて作成した計6層構造からなるナノチューブの外径は約400 nm，内径は約300 nm，管壁厚は約50 nmとなる（Fig. 7）．鋳型内交互積層法（テンプレート合成）の利点は，

① 電荷を有する水溶性分子（蛋白質，生体分子，高分子電解質など）であれば，ナノチューブの素材になり得る（分子設計の自由度が高く，構成分子の選択範囲が広い）
② 鋳型となる多孔性膜の孔径および厚みの調節により，チューブの外径および長さを均一に制御することができる
③ 積層膜数の調節により，チューブの内径をナノメートルスケールで制御することができる
④ 複数の機能性分子を任意の順序で積層することにより，管壁構造を自由に分子設計できる
⑤ 他のナノチューブ合成法に比べ，調製が簡便，再現性が高く，低コスト，大型化が容易

などである．

得られたナノチューブの最大の特徴は，同重量の球状構造体

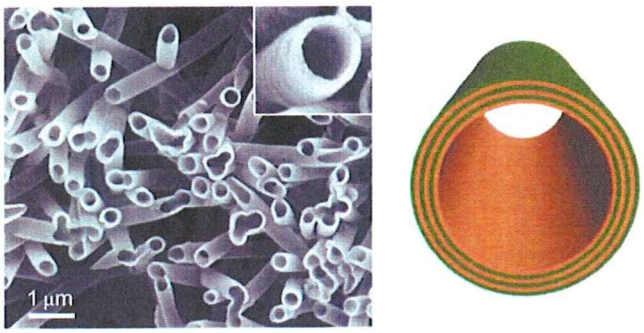

Fig. 7. SEM images of protein nanotubes comprised of $(PLA/HSA)_3$. Schematic illustration of the protein nanotubes prepared by template synthesis using layer-by-layer deposition technique.

に比べて比表面積が大きいことにある．HSAナノチューブの水分散液にHSAのリガンド（薬物など）を添加すると，ナノチューブ管壁に効率よく結合し，水中から速やかに除去される．HSAに結合しない分子は全く取り込まれないので，いつまでも水中に存在する．HbやMbを構成成分としてナノチューブを作成することもできるし[57]，HSA-FePからなるナノチューブは酸素を可逆的に吸脱着する[55]．また，最終層成分の選定だけで内孔に合目的な特性を付与することができるので，例えば最内層に加水分解酵素を配置したHSAナノチューブでは，内孔壁表面で基質の加水分解が進行する．逆に酵素合成により新物質を創り出すこともできる．まさにナノサイズのリアクターである．この場合，内孔以外の管壁を構成する蛋白質がHSAであることが肝要である．他にも鉄イオンの捕捉・貯蔵を担う球殻状蛋白質フェリチンからなるナノチューブも合成され，バイオナノデバイスとして磁化特性，半導体特性が検討されている．

管壁のみならず，チューブの一次元内孔空間にウイルスやリポソームなどの大きな生体超分子をサイズ選択的に捕捉することも可能である．中空シリンダーの両端開口部が自由に開閉できれば，従来のミセルやリポソームとは全く違う新しいドラッグキャリアの誕生にもつながるであろう．

8．おわりに

筆者らはヒト血清アルブミンの多分子結合能に着目し，その内部に機能性分子を取り込ませる方法により，数々の人工蛋白質を創製してきている．当初は酸素運搬体に焦点を絞った展開であったが，合成ヘムのみならず他の機能性分子も効率よく包接できることがわかり，水の還元による水素発生や一重項酸素生成の光増感剤となるアルブミンを開発した．実は多分子結合能のみならず，きわめて高い水溶性や光・熱に対する安定性といった血清蛋白質アルブミンならではの特徴が，これらの新物質系において重要な役割を果たしている．さらに，遺伝子組換え技術を駆使してアルブミンのアミノ酸配置を少しだけ変えてやると，機能制御が可能になることも明らかにした．X線結晶構造解析（生物物理学）にもとづいた部位特異的アミノ酸置換（分子生物学）を機能性アルブミン開発の分子設計に取り入れ，新しい方法論として定着させた．最近はアルブミンからなる中空シリンダー構造のナノチューブを合成し，その機能展開に力を入れているが，ここでもアルブミンの高い構造安定性が大きく貢献している．ウイルス捕捉，標的薬物の結合・放出，ナノリアクター，ナノバイオデバイスなど，多くの応用展開が期待される．

謝　辞

本総説は，日本学術振興会科学研究費補助金，科学技術振興機構戦略的創造研究推進事業“さきがけ”，厚生労働省科学研究費補助金の支援により推進された研究の成果である．遺伝子組換え蛋白質の合成，X線結晶構造解析はProf. Stephen Curry（Imperial College London）の協力のもと行われた．動物実験は小林紘一教授（慶大医），堀之内宏久准教授（慶大医）の協力を得て実施された．また，試料調製・生化学実験は小林　直（早大理工研），寺田裕美（早大理工研）が担当した．ここに記して謝意を表する．

引用文献

1. Peters T. All about Albumin: Biochemistry, Genetics and Medical Applications. San Diego: Academic Press, 1996; and references therein.
2. Kragh-Hansen U. Molecular aspects of ligand binding to serum albumin. Pharmacol Rev 1981;33:17-53.
3. Kragh-Hansen U. Structure and ligand-binding properties of human serum-albumin. Danish Med Bull 1990;37:57-84.
4. He XM, Carter DC. Atomic structure and chemistry of human serum albumin. Nature 1992;358:209-215.
5. Sudlow G, Birkett DJ, Wade DN. The characterization of two specific drug binding sites on human serum albumin. Mol Pharmacol 1975;11:824-832.
6. Kobayashi K. Summary of recombinant human serum albumin development. Biologicals 2006;34:55-59.
7. Mahammed A, Gross Z. Albumin-conjugated corrole metal complexes: extremely simple yet very efficient biomimetic oxidation Systems. J Am Chem Soc 2005;127:2883-2887.
8. Reetz MT, Jiao N. Copper-phthalocyanine conjugates of serum albumins as enantioselective catalysts in Diels-Alder reactions. Angew Chem Int Ed 2006;45:2416-2419.
9. Curry S, Madelkow H, Brick P, Franks N. Crystal structure of human serum albumin complexed with fatty acid reveals an asymmetric distribution of binding sites. Nat Struct Biol 1998;5:827-835.
10. Curry S, Brick P, Franks N. Fatty acid binding to human serum albumin: new insights from crystallographic studies. Biochim Biophys Acta 1999;1441:131-140.
11. Simard JR, Zunszain PA, Hamilton JA, Curry S. Location of high and low affinity fatty acid binding sites on human

serum albumin revealed by NMR drug-competition analysis. J Mol Biol 2006;361:336-351.
12. Petitpas I, Petersen CE, Ha CE, Bhattacharya AA, Zunszain PA, Ghuman J, Bhagavan NV, Curry S. Structural basis of albumin-thyroxine interactions and familial dysalbuminemic hyperthyroxinemia. Proc Natl Acad Sci USA 2003;100:6440-6445.
13. Ghuman J, Zunszain PA, Petotpas I, Bhattacharya AA, Otagiri M, Curry S. Structural basis of the drug-binding specificity of human serum albumin. J Mol Biol 2005;353:38-52.
14. Zunszain PA, Ghuman J, McDonagh AF, Curry S. Crystallographic analysis of human serum albumin complexed with 4Z,15E-biririubin-IXα. J Mol Biol 2008;381: 394-406.
15. Komatsu T, Hamamatsu K, Wu J, Tsuchida E. Physicochemical properties and O_2-coordination structure of human serum albumin incorporating tetrakis (o-pivalamido) phenylporphinatoiron (II) derivatives. Bioconjugate Chem 1999;10:82-86.
16. Tsuchida E, Komatsu T, Mastukawa Y, Hamamatsu K, Wu J. Human serum albumin incorporating tetrakis (o-pivalamido) phenylporphinatoiron (II) derivative as a totally synthetic O_2-carrying hemoprotein. Bioconjugate Chem 1999;10:797-802.
17. Komatsu T, Matsukawa Y, Tsuchida E. Kinetics of CO and O_2 binding to human serum albumin-heme hybrid. Bioconjugate Chem 2000;11:772-776.
18. Komatsu T, Matsukawa Y. Tsuchida E. Reaction of nitric oxide with synthetic hemoprotein, human serum albumin incorporating tetraphenylporphinatoiron (II) derivatives. Bioconjugate Chem. 2001;12:71-75.
19. Komatsu T, Okada T, Moritake M, Tsuchida E. O_2-binding properties of double-sided porphinatoiron (II) s with polar substituents and their human serum albumin hybrids. Bull Chem Soc Jpn 2001;74:1695-1702.
20. Komatsu T, Matsukawa Y, Tsuchida E. Effect of heme structure on O_2-binding properties of human serum albumin-heme hybrids: intramolecular histidine coordination provides a stable O_2-adduct complex. Bioconjugate Chem 2002;13:397-402.
21. Nakagawa A, Komatsu T, Iizuka M, Tsuchida E. Human serum albumin hybrid incorporating tailed porphyrinatoiron (II) in the $\alpha,\alpha,\alpha,\beta$-conformer as an O_2-binding site. Bioconjugate Chem 2006;17:146-151.
22. Nakagawa A, Komatsu T, Iizuka M, Tsuchida E. O_2 binding to human serum albumin incorporating iron porphyrin with a covalently linked methyl-L-histidine isomer. Bioconjugate Chem 2008;19:581-584.
23. Komatsu T, Huang Y, Wakamoto S, Abe H, Fujihara M, Azuma H, Ikeda H, Yamamoto H, Horinouchi H, Kobayashi K, Tsuchida E. Influence of O_2-carrying plasma hemoprotein "albumin-heme" on complement system and platelet activation in vitro and physiological responses to exchange transfusion. J Biomed Mater Res 2007;81A:821-826.
24. Tsuchida E, Komatsu T, Yanagimoto T, Sakai H. Preservation stability and in vivo administration of albumin-heme hybrid solution as an entirely synthetic O_2-carrier. Polym Adv Technol 2002;13:845-850.
25. Tsuchida E, Komatsu T, Hamamatsu K, Matsukawa Y, Tajima A, Yoshizu A, Izumi Y, Kobayashi K. Exchange transfusion of albumin-heme as an artificial O_2-infusion into anesthetized rats: physiological responses, O_2-delivery and reduction of the oxidized hemin sites by red blood cells. Bioconjugate Chem 2000;11:46-50.
26. Komatsu T, Yamamoto H, Huang Y, Horinouchi H, Kobayashi K, Tsuchida E. Exchange transfusion with synthetic oxygen-carrying plasma protein "albumin-heme" into an acute anemia rat model after seventy-percent hemodilution. J Biomed Mater Res 2004;71A:644-651.
27. Tsuchida E, Komatsu T, Matsukawa Y, Nakagawa Y, Sakai H, Kobayashi K, Suematsu M. Human serum albumin incorporating synthetic heme: red blood cell substitute without hypertension by nitric oxide scavenging. J Biomed Mater Res 2003;64A:257-261.
28. Kobayashi K, Komatsu T, Iwamaru A, Matsukawa Y, Watanabe M, Horinouchi H, Tsuchida E. Oxygenation of hypoxia region in solid tumor by administration of human serum albumin incorporating synthetic hemes. J Biomed Mater Res 2003;64A:48-51.
29. Linberg R, Conover CD, Shum KL, Shorr RGL. Increased tissue oxygenation and enhanced radiation sensitivity of solid tumors in rodents following polyethylene glycol conjugated bovine hemoglobin administration. In Vivo 1998;12:167-174.
30. Horinouchi H, Yamamoto H, Komatsu T, Huang Y, Tsuchida E, Kobayashi K. Enhanced radiation response of a solid tumor with the artificial oxygen carrier 'albumin-heme'. Cancer Sci 2008;99:1274-1278.
31. Huang Y, Komatsu T, Wang RM, Nakagawa A, Tsuchida E. Poly (ethylene glycol)-conjugated human serum albumin including iron porphyrins: surface modification improves the O_2-transporting ability. Bioconjugate Chem 2006;17:393-398.
32. Huang Y, Komatsu T, Yamamoto H, Horinouchi H, Kobayashi K, Tsuchida E. PEGylated albumin-heme as an oxygen-carrying plasma expander: exchange transfusion

into acute anemia rat model. Biomaterials 2006;27:4477-4483.
33. Komatsu T, Ohmichi N, Zunszain PA, Curry S, Tsuchida E. Dioxygenation of human serum albumin having a prosthetic heme group in a tailor-made heme pocket. J Am Chem Soc 2004;126:14304-14305.
34. Paoli M. Anderson BF, Baker HM, Morgan WT, Smith A, Baker EN. Crystal structure of hemopexin reveals a novel high-affinity heme site formed between two β-propella domains. Nat Struct Biol 1999;6:926-931.
35. Fairley NH. Methemalbumin (pseudo-methemoglobin). Nature 1938;142:1156-1157.
36. Muller-Eberhard U, Morgan WT. Porphyrin-binding proteins in serum. Ann NY Acad Sci 1975;244:624-650.
37. Adams PA, Berman MC. Kinetics and mechanism of the interaction between human serum albumin and monomeric haemin. Biochem J 1980;191:95-102.
38. Wardell M, Wang Z, Ho JX, Robert J, Ruker F, Rubel J, Carter DC. The atomic structure of human serum methemalbumin at 1.9 Å. Biochem Biophys Res Commun 2002;291:813-819.
39. Zunszain PA, Ghuman J, Komatsu T, Tsuchida E, Curry S. Crystal structural analysis of human serum albumin complexed with hemin and fatty acid. BMC Struct Biol 2003;3:6.
40. Komatsu T, Ohmichi N, Nakagawa A, Zunszain PA, Curry S, Tsuchida E. O_2 and CO binding properties of artificial hemoproteins formed by complexing iron protoporphyrin IX with human serum albumin mutants. J Am Chem Soc 2005;127:15933-15942.
41. Phillips SEV, Schoenborn BP. Neuteon diffraction reveals oxygen-histidine hydrogen bond in oxymyoglobin. Nature 1981;292:81-82.
42. Shaanan B. Structure of human oxyhemoglobin at 2.1 Å resolution. J Mol Biol 1983;171:31-59.
43. Komatsu T, Nakagawa A, Zunszain PA, Curry S, Tsuchida E. Genetic engineering of the heme pocket in human serum albumin: modulation of O_2 binding of iron protoporphyrin IX by variation of distal amino acids. J Am Chem Soc 2007;129:11286-11295.
44. Kalyanasundaram K, Grätzel M. Light induced redox reactions of water soluble porphyrins, sensitization of hydrogen generation from water by zincporphyrin derivatives. Helv Chim Acta 1980;63:478-485.
45. Komatsu T, Wang RM, Zunszain PA, Curry S, Tsuchida E. Photosensitized reduction of water to hydrogen using human serum albumin complexed with zinc-protoporphyrin IX. J Am Chem Soc 2006;128:16297-16301.
46. Dougherty TJ. Studies on the structure of porphyrins contained in Photofrin-II. Photochem Photobiol 1987;46:569-573.
47. Dougherty TJ, Gomer CJ, Henderson BW, Jori G, Kessel D, Korbelik M, Moan J, Peng Q. Photodynamic therapy. J Natl Cancer Inst 1998;90:889-905.
48. Lopez RFV, Lange N, Guy R, Bentley MVLB. Photodynamic therapy of skin cancer: controlled drug delivery of 5-ALA and its esters. Drug Deliver Rev 2004;56:77-94.
49. Aveline B, Hasen T, Redmond RW. Photophysical and photosensitizing properties of benzoporphyrin derivative monoacid ring A (BPD-MA). Photochem Photobiol 1994;59:328-335.
50. Guldi DM, Prato M. Excited-state properties of C_{60} fullerene derivatives. Acc Chem Res 2000;33:695-703.
51. Arbogast JW, Darmanyan AP, Foote CS, Rubin Y, Diederich FN, Alvarez MM, Anz SJ, Whetten RL. Photophysical properties of C_{60}. J Phys Chem 1991;95:11-12.
52. Anderson JL, An YZ, Rubin Y, Foote CS. Photophysical characterization and single oxygen yield of a dihydrofullerene. J Am Chem Soc 1994;116:9763-9764.
53. Qu X, Komatsu T, Sato T, Glatter O, Horinouchi H, Kobayashi K, Tsuchida E. Structure, photophysical property, and cytotoxicity of human serum albumin complexed with tris (dicarboxymethylene)[60]fullerene. Bioconjugate Chem 2008;19:1556-1560.
54. Wilkinson F, Helman WP, Rossa AB. Quantum yields for the photosensitized formation of the lowest electronically excited singlet-state of molecular-oxygen in solution, J Phys Chem Ref Data 1993;22:113-262.
55. Lu G, Komatsu T, Tsuchida E. Artificial hemoprotein nanotubes. Chem Commun 2007;2980-2982.
56. Lu G, Tsuchida E, Komatsu T. Human serum albumin nanotubes comprising layer-by-layer assembly with polycation. Chem Lett 2008;37:972-973.
57. Qu X, Lu G, Tsuchida E, Komatsu T. Protein nanotubes comprised of an alternate layer-by-layer assembly using a polycation as an electrostatic glue. Chem Eur J 2008;14:10303-10308.

O_2 Binding Properties of Human Serum Albumin Quadruple Mutant Complexed Iron Protoporphyrin IX with Axial His-186 Coordination

Akito Nakagawa,[1] Teruyuki Komatsu,*[1,2] Stephen Curry,[3] and Eishun Tsuchida[1]
[1]*Research Institute for Science and Engineering, Waseda University, 3-4-1 Okubo, Shinjuku-ku, Tokyo 169-8555*
[2]*PRESTO, Japan Science and Technology Agency (JST), 4-1-8 Honcho, Kawaguchi 332-0012*
[3]*Biophysics Section, Blackett Laboratory, Imperial College London, Exhibition Road, London SW7 2AZ, U.K.*

(Received May 18, 2009; CL-090494; E-mail: teruyuki@waseda.jp)

The O_2 binding properties of complexes of iron(II) protoporphyrin IX with quadruple mutants of recombinant human serum albumin (rHSA) that provide axial His-186 coordination have been characterized; their O_2 binding parameters were similar to those of analogues having proximal His-185 and of human red blood cells.

In our bloodstream, iron(III) protoporphyrin IX (hemin) dissociated from methemoglobin (metHb) is captured by human serum albumin (HSA) and transported to liver cells for catabolism. Crystal structure analysis of this naturally occurring hemoprotein revealed that hemin is bound within a narrow D-shaped cavity in subdomain IB of HSA with a weak axial coordination by Tyr-161 and electrostatic interactions between the porphyrin propionate side-chains and three basic amino acid residues (Arg-114, His-146, and Lys-190) (Figure 1).[1,2] The axial phenolate ligation by Tyr-161 of HSA keeps the hemin group physiologically silent. In fact, the reduced ferrous HSA–heme is immediately oxidized by O_2.[3] We previously demonstrated that a pair of site-specific mutations in subdomain IB of HSA conferred O_2 binding capability on the heme: (i) introduction of a proximal His at Leu-185 position and (ii) substitution of Tyr-161 with noncoordinating Leu.[4a,4b] The resulting artificial hemoprotein can reversibly bind O_2 in much the same way as Hb and myoglobin (Mb). The albumin-based O_2 carrier has attracted medical interest because of its potential acting as a red blood cell (RBC) substitute. Interestingly, the proximal His introduced into the opposite side of the porphyrin plane (Ile-142 position) also allows O_2 binding to the heme.[4] These results suggest that there may be other sites where the proximal His can be inserted in the coordination sphere of the central iron. Our modeling and experimental results showed that Arg-186 is the third candidate because rHSA(I142H/Y161L/R186H)–heme formed a bishistidyl low-spin hemochrome.[4c] Furthermore, we have recently found that replacing His-146 and Lys-190 at the entrance of the heme pocket with Arg (H146R, K190R) resolved the structural heterogeneity of the two orientations of the porphyrin plane and afforded a single O_2 binding affinity.[4d]

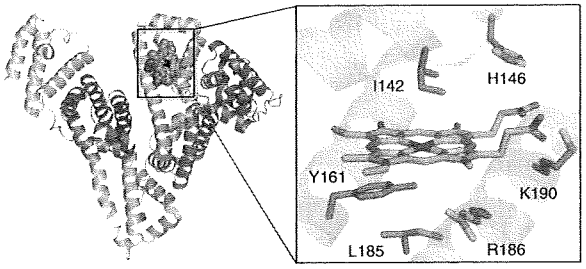

rHSA	Position				
	146	161	185	186	190
Wild type (wt)	His	Tyr	Leu	Arg	Lys
H146R/Y161G/R186H/K190R (1G)	**Arg**	**Gly**	Leu	**His**	**Arg**
H146R/Y161L/R186H/K190R (1L)	**Arg**	**Leu**	Leu	**His**	**Arg**
H146R/Y161G/L185H/K190R (2G)	**Arg**	**Gly**	**His**	Arg	**Arg**
H146R/Y161L/L185H/K190R (2L)	**Arg**	**Leu**	**His**	Arg	**Arg**

Figure 1. Structure of the heme pocket in the rHSA(wt)–hemin complex (PDB ID: 1O9X from ref 2).[5] Positions of the amino acids where site-specific mutations were introduced and abbreviations of the mutants are shown in the table. Structural models of the four rHSA(quadruple mutant)–heme complexes are demonstrated in Figure S1.[5,6]

In this study, we generated new rHSA(quadruple mutant)–heme complexes involving axial His-186 coordination and kinetically characterized their O_2 binding properties. The steric effect of the neighboring amino acid at the 161 position to the O_2 binding parameters is also investigated.

We designed rHSA quadruple mutants; rHSA(H146R/Y161G/R186H/K190R) [rHSA**1**G], rHSA(H146R/Y161L/R186H/K190R) [rHSA**1**L], rHSA(H146R/Y161G/L185H/K190R) [rHSA**2**G], and rHSA(H146R/Y161L/L185H/K190R) [rHSA**2**L] (Figure 1). Site-specific mutations were introduced into the HSA coding region in a plasmid vector (pHIL-D2 HSA) using the QuikChange (Stratagene) mutagenesis kit. All mutations were confirmed by DNA sequencing. The proteins were expressed in the yeast species *Pichia pastoris*. The corresponding ferric rHSA–hemin complexes were prepared according to our previously reported procedures.[4]

UV–vis absorption spectra of the four rHSA(quadruple mutant)–hemin complexes were essentially identical regarding their general features (Figure 2, Table S1).[6] They were easily reduced to the ferrous complexes by adding a small molar excess of aqueous $Na_2S_2O_4$ under an N_2 atmosphere (Figure S1).[6] A broad absorption band (λ = 557–559 nm) in the visible region was similar to that observed for deoxy Mb, indicating the formation of a five-N-coordinate high-spin ferrous complex.[7,8] Upon exposure of the rHSA–heme solution to O_2, the UV–vis absorption changed to that of the O_2 adduct complex (Figure 2).[4,7,8] After flowing CO gas, these hemoproteins produced stable carbonyl complexes. It can be concluded that the histidyl group at position 186 acts as a proximal base for dioxygenation of the prosthetic heme group. In contrast, rHSA(single mutant)–heme [rHSA(L185H)–heme and rHSA(R186H)–heme] could not bind O_2. In these complexes, Tyr-161 appears to coordinate to the central ferrous ion of the heme in competition with His-186 or His-185.

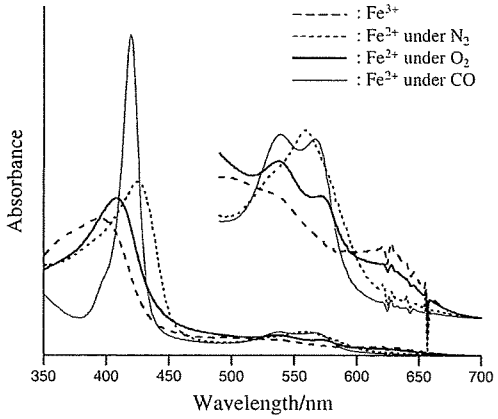

Figure 2. UV–vis. absorption spectral changes of rHSA1L–heme in 50 mM potassium phosphate buffered solution (pH 7.0) at 22 °C.

To determine the association and dissociation rate constants (k_{on} and k_{off}) for O_2 binding to rHSA(quadruple mutant)–heme, laser flash photolysis experiments were carried out.[4b] The O_2 recombination to the heme after the laser pulse irradiation occurs according to eq 1.

$$\text{Heme} + O_2 \underset{k_{off}}{\overset{k_{on}}{\rightleftarrows}} \text{Heme-}O_2 \qquad (1)$$

$$[P_{1/2} = K^{-1} = (k_{on}/k_{off})^{-1}]$$

The time dependences of the absorbance decays accompanying the O_2 and CO recombinations to rHSA(quadruple mutant)–heme complexes were clearly monophasic (Figure S2).[6] This can be attributed to a uniform heme orientation in the subdomain IB by introduction of Arg into the His-146 and Lys-190 positions.[4] As a result, each hemoprotein showed a single O_2 binding affinity (Table 1). It is noteworthy that all the rHSA(quadruple mutant)–heme complexes exhibited similar O_2 binding parameters independent of the position of the axial base (His-185 or His-186) and the size of the hydrophobic amino acid residue at 161 (Gly or Leu). We had postulated that the small Gly-161 would provide greater room for the proximal His-186 (or His-185), thereby loosening the spatially confined axial ligation. In general, such fluctuation decreases the k_{off} value and enhances the O_2 binding.[4b,4c] However, this was not observed in dioxygenation of rHSA1G–heme and rHSA2G–heme. The O_2 binding affinities ($P_{1/2}$) of the rHSA(quadruple mutant)–heme complexes (5–8 Torr) are very close to that of the human RBC ($P_{1/2}$ = 8 Torr) and, therefore, well adapted for O_2 transport in the circulatory system.

In conclusion, we have prepared rHSA(quadruple mutant)–heme complexes, in which (i) the proximal His was introduced at position 186 (or 185), (ii) Tyr-161 was substituted with Gly or Leu, and (iii) His-146 and Lys-190 at the heme pocket entrance were replaced with Arg. These artificial hemoproteins formed O_2 adduct complexes with a similar O_2 binding affinity. On the basis of our systematic investigations on rHSA–heme,[4] we conclude that the favorable positions for proximal His insertion are 142, 185, and 186; in all cases Tyr-161 must be replaced with noncoordinating amino acid (e.g., Gly, Leu, Phe, though Ala, Val, or Ile may also be tolerated). This structural flexibility of the heme pocket architecture in HSA has enabled the creation not only of an artificial O_2 carrier using the most abundant plasma protein but may also allow engineering of various hemoprotein enzymes.

Table 1. O_2 binding parameters of rHSA(quadruple mutant)–heme in 50 mM potassium phosphate buffered solution (pH 7.0) at 22 °C

Hemoproteins	k_{on} /μM^{-1} s^{-1}	k_{off} /ms^{-1}	$P_{1/2}$ /Torr
rHSA1G–heme	39	0.36	6
rHSA1L–heme	67	0.54	5
rHSA2G–heme	36	0.46	8
rHSA2L–heme[a]	42	0.41	6
Hbα (R-state)	33[b]	0.013[c]	0.24
Mb[d]	14	0.012	0.51
RBC[e]			8

[a]Ref 4d. [b]In 0.1 M phosphate buffer (pH 7.0, 21.5 °C), ref 9. [c]In 10 mM phosphate buffer (pH 7.0, 20 °C), ref 10. [d]In 0.1 M phosphate buffer (pH 7.0, 20 °C), ref 11. [e]Human RBC suspension, in isotonic buffer (pH 7.4, 20 °C), ref 12.

This work was partially supported by Grant-in-Aid for Scientific Research (No. 20750142 and No. 20350058) from JSPS, PRESTO from JST, and Health Science Research Grants from MHLW Japan.

References and Notes

1 M. Wardell, Z. Wang, J. X. Ho, J. Robert, F. Ruker, J. Ruble, D. C. Carter, *Biochem. Biophys. Res. Commun.* **2002**, *291*, 813.
2 P. A. Zunszain, J. Ghuman, T. Komatsu, E. Tsuchida, S. Curry, *BMC Struct. Biol.* **2003**, *3*, 6.
3 E. Monzani, B. Bonafe, A. Fallarrini, C. Redaelli, L. Casella, L. Minchiotti, M. Galliano, *Biochim. Biophys. Acta* **2001**, *1547*, 302.
4 a) T. Komatsu, N. Ohmichi, P. A. Zunszain, S. Curry, E. Tsuchida, *J. Am. Chem. Soc.* **2004**, *126*, 14304. b) T. Komatsu, N. Ohmichi, A. Nakagawa, P. A. Zunszain, S. Curry, E. Tsuchida, *J. Am. Chem. Soc.* **2005**, *127*, 15933. c) T. Komatsu, A. Nakagawa, P. A. Zunszain, S. Curry, E. Tsuchida, *J. Am. Chem. Soc.* **2007**, *129*, 11286. d) Nakagawa, T. Komatsu, S. Curry, E. Tsuchida, *Org. Biomol. Chem.* **2009**, *7*, in press.
5 The picture was produced using PyMOL, W. L. DeLano, *The PyMOL Molecular Graphics System*, DeLano Scientific, San Carlos, CA, **2002**.
6 Supporting Information is available electronically on the CSJ-Journal Web site, http://www.csj.jp/journals/chem-lett/index.html.
7 E. Antonini, M. Brunori, *Hemoglobin and Myoglobin in Their Reactions with Ligands*, North-Holland Pub. Com., Amsterdam, **1971**, p. 18.
8 T. G. Traylor, C. K. Chang, J. Geibel, A. Berziniz, T. Mincey, J. Cannon, *J. Am. Chem. Soc.* **1979**, *101*, 6716.
9 Q. H. Gibson, *J. Biol. Chem.* **1970**, *245*, 3285.
10 J. S. Olson, M. E. Andersen, Q. H. Gibson, *J. Biol. Chem.* **1971**, *246*, 5919.
11 R. Rohlfs, A. J. Mathews, T. E. Carver, J. S. Olson, B. A. Springer, K. D. Egeberg, S. G. Sligar, *J. Biol. Chem.* **1990**, *265*, 3168.
12 K. Imai, H. Morimoto, M. Kotani, H. Watari, W. Hirata, M. Kuroda, *Biochim. Biophys. Acta* **1970**, *200*, 189.

Published on the web (Advance View) June 27, 2009; doi:10.1246/cl.2009.776

Am J Physiol Heart Circ Physiol 297: H905–H910, 2009.
First published July 2, 2009; doi:10.1152/ajpheart.00430.2009.

TRANSLATIONAL PHYSIOLOGY

Hemoglobin vesicles improve wound healing and tissue survival in critically ischemic skin in mice

Jan A. Plock,[1,2] Nassim Rafatmehr,[2] Dubravko Sinovcic,[2] Jonas Schnider,[2] Hiromi Sakai,[3] Eishun Tsuchida,[3] Andrej Banic,[1] and Dominique Erni[1,2]

[1]*Department of Plastic and Hand Surgery, Inselspital, and* [2]*Department of Clinical Research, University of Bern, Bern, Switzerland; and* [3]*Research Institute for Science and Engineering, Waseda University, Tokyo, Japan*

Submitted 7 May 2009; accepted in final form 29 June 2009

Plock JA, Rafatmehr N, Sinovcic D, Schnider J, Sakai H, Tsuchida E, Banic A, Erni D. Hemoglobin vesicles improve wound healing and tissue survival in critically ischemic skin in mice. *Am J Physiol Heart Circ Physiol* 297: H905–H910, 2009. First published July 2, 2009; doi:10.1152/ajpheart.00430.2009.—Local hypoxia, as due to trauma, surgery, or arterial occlusive disease, may severely jeopardize the survival of the affected tissue and its wound-healing capacity. Initially developed to replace blood transfusions, artificial oxygen carriers have emerged as oxygen therapeutics in such conditions. The aim of this study was to target primary wound healing and survival in critically ischemic skin by the systemic application of left-shifted liposomal hemoglobin vesicles (HbVs). This was tested in bilateral, cranially based dorsal skin flaps in mice treated with a HbV solution with an oxygen affinity that was increased to a P_{50} (partial oxygen tension at which the hemoglobin becomes 50% saturated with oxygen) of 9 mmHg. Twenty percent of the total blood volume of the HbV solution was injected immediately and 24 h after surgery. On the first postoperative day, oxygen saturation in the critically ischemic middle flap portions was increased from 23% (untreated control) to 39% in the HbV-treated animals ($P < 0.05$). Six days postoperatively, flap tissue survival was increased from 33% (control) to 57% ($P < 0.01$) and primary healing of the ischemic wound margins from 6.6 to 12.7 mm ($P < 0.05$) after HbV injection. In addition, higher capillary counts and endothelial nitric oxide synthase expression (both $P < 0.01$) were found in the immunostained flap tissue. We conclude that left-shifted HbVs may ameliorate the survival and primary wound healing in critically ischemic skin, possibly mediated by endothelial nitric oxide synthase-induced neovascularization.

artificial blood; surgical flap; hypoxia; microcirculation; necrosis

OXYGEN DELIVERY to a certain tissue compartment is defined by the product of volumetric blood flow and oxygen content in the arterial inflow. If blood perfusion is reduced, as due to injury to the feeding vessels or arterial occlusive disease, critical ischemia and subsequent cellular hypoxia may occur, which may eventually lead to gangrene predominantly in the most remote areas. In addition, it has been repeatedly shown that wound healing in such critically ischemic skin may be impaired, which results in considerable morbidity, i.e., chronic wounds, delayed wound healing after surgery, and secondary wound infection (10).

The primary therapeutic strategy in such conditions is aimed at reestablishing the interrupted vascular axis by means of surgical or endovascular interventions. However, adjunct measures may be required if this is not possible or successful, such as due to anatomical reasons or the patient's general health constitution. A possible strategy would be to provide such patients with supplementary oxygen to promote essential oxygen-dependent processes in wound healing, such as fibroblast proliferation, neovascularization, and collagen synthesis (9).

Recently, an alternative method to improve oxygenation in critically ischemic tissue has emerged, which consists in the use of artificial oxygen carriers, such as perfluorocarbons and hemoglobin (Hb)-based compounds. These biomaterials have been initially developed to avoid the drawbacks of blood transfusions including immunologic reactions, blood-borne transmitted infections, limited availability, and restricted storage time (4). More than mere blood substitutes, the artificial oxygen carriers may be considered as oxygen therapeutics augmenting oxygen distribution to tissues in need (25).

In a series of previous studies, we have investigated the efficacy of liposomal Hb vesicles (HbVs) in critically ischemic skin in an acute hamster flap model (5, 6, 8, 17, 18). Substantial improvements in oxygenation, oxidative energy metabolism, microcirculatory blood flow, and hypoxia-related inflammation and apoptosis were demonstrated. Furthermore, we have observed that the performance of the HbVs was enhanced by raising their oxygen affinity (shifting the oxygen dissociation curve to the left) (5, 6).

Based on these extensive physiological studies, we intended to evaluate the biological efficiency of high-oxygen affinity HbVs in terms of the survival and healing capacity of critically ischemic tissue. This was tested in a chronic skin flap in mice, in which tissue survival and primary wound healing were impaired due to critical ischemia. In addition, we investigated a possible involvement of endothelial nitric oxide synthase (eNOS) expression and neovascularization in the postulated HbV effect.

MATERIALS AND METHODS

Vesicle solutions. The HbVs were prepared as previously reported (19, 20). Briefly, Hb was purified from outdated donated blood and encapsulated with a phospholipid bilayer membrane coated with polyethylene glycol. The diameter of the HbVs was ~250 nm, and the Hb concentration inside the vesicle was 35 g/dl. The Hb oxygen affinity was regulated to a P_{50} (partial oxygen tension at which the hemoglobin becomes 50% saturated with oxygen) of 9 mmHg without a coencapsulation of an allosteric effector. The HbVs were suspended in 0.9% NaCl at a final Hb concentration of 10 g/dl. To determine the

Address for reprint requests and other correspondence: J. A. Plock, Dept. of Plastic and Hand Surgery, Inselspital, Univ. of Bern, CH-3010 Bern, Switzerland (e-mail: jan.plock@insel.ch).

pharmacokinetic behavior of the vesicles, a sulforhodamine B solution (10 mM, Invitrogen, Tokyo, Japan) was encapsulated instead of Hb. The two types of vesicles featured otherwise identical physicochemical properties.

Animals, experimental groups, and flap preparation. The experiments were performed according to the National Institutes of Health guidelines for the care and use of laboratory animals and with the approval of the local Animal Ethics Committee. Forty-eight DDY mice weighing 22 to 26 g were included in this study. Eighteen animals were used for assessing the pharmacokinetics and plasma viscosity; the others were randomly assigned and equally distributed to an untreated control group and to groups receiving either 0.9% NaCl or HbVs.

The anesthetized animals were placed on a heating pad in a prone position, and the room temperature was set at 28°C to keep the animal's skin temperature constant at 32°C, which was verified with a microthermometer placed on the abdominal skin. The back skin was shaved and epilated. Surgery was performed with the aid of an operating microscope at ×10 magnification (Wild, Heerbrugg, Switzerland). Two cranially based flaps measuring 30 × 15 mm were dissected on both sides of the dorsal midline (Fig. 1). The flaps consisted of skin, a thin layer of panniculus carnosus muscle, and subcutaneous tissue. The lateral thoracic artery was ligated, thus creating random collateral arterial perfusion of the flap via the subdermal vascular plexus. During surgery, the flap was irrigated with 0.9% NaCl to prevent it from drying out. The flaps were sutured back into their original position after having placed a silicone sheet underneath to avoid vascular ingrowth from the wound bed.

Tissue oxygenation. Cutaneous oxygen saturation was measured with a noninvasive microprobe system performing white light spectrometry for computed data collection (O2C-system. LEA-Medizintechnik, Giessen, Germany). According to the manufacturer, the sample surface and depth were ~1 mm^2 and 800 μm, respectively. Probes were placed on the neck (normal skin) and in the central flap axis at distances of 5 (proximal flap), 15 (middle flap), and 25 mm (distal flap) from the base of the flap.

Tissue survival and primary wound healing. The length of the healed wound suture was measured in the midline (ischemic flap tissue sutured to each other) and laterally (ischemic flap tissue sutured to healthy tissue). A digital photographic picture was taken of both flaps, which was computerized for planimetry to calculate the percentage of the total flap surface that became necrotic (Adobe Photoshop, Adobe, San Jose, CA).

Histological examination. Tissue samples were taken from the spleen, liver, and kidney, which are where the HbVs are degraded by the reticuloendothelial system and excreted (20). In addition, specimens were harvested from the flap tissue at a standardized distance to the flap basis of 5 mm. This region was chosen to obtain healthy flap tissue well off the inflamed demarcation zone or necrosis. The samples were fixed in 4% paraformaldehyde, washed in PBS, stored in 70% ethanol, and finally embedded in paraffin blocks. Sections (5 μm) were cut, transferred to microslides, and air dried at 37°C overnight. Hematoxylin-eosin staining was performed for morphological evaluation and Giemsa staining for visualizing leukocytes. In addition, the flap tissue specimens were immunohistochemically stained for eNOS. To this end, peroxidase was blocked with 3% H_2O_2, and nonspecific reactions were reduced by protein blocking (DakoCytomation, Protein Block, Serum-Free, Zug, Switzerland). The slides were then incubated with a primary rabbit anti-eNOS antibody (1:50; Santa Cruz, Heidelberg, Germany). The anti-rabbit EnVision (DakoCytomation EnVision+ System Labelled Polymer-HRP Anti-Rabbit K4003) and AEC (Aminoethyl Carbazole Substrate Kit, Zymed, San Francisco, CA) were used as secondary antibody and chromogen, respectively. Positive and negative controls were taken for each set of antibody and between each step. Immunostaining was assessed semiquantitatively by using light microscopy at a ×200 magnification (Leica DM7RB, Wetzlar, Germany). The total numbers of capillaries and eNOS positive capillaries within one visual field were counted. Data were calculated from the averages of three randomly selected visual fields per specimen.

Laboratory analysis. Hb and methemoglobin (met-Hb) concentrations were analyzed in the blood samples (ABL 625; Radiometer, Copenhagen, Denmark). The samples were centrifuged with 3,000 rounds/min for 10 min to determine hematocrit and to obtain the plasma. Since the HbVs are known to be part of the plasma (20), the

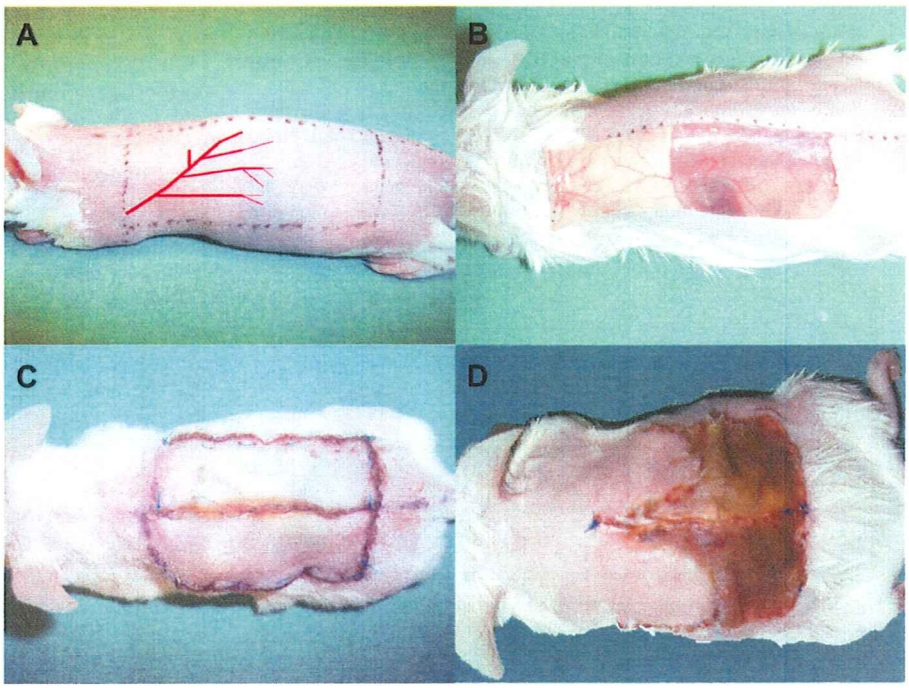

Fig. 1. Experimental model. *A* and *B*: a cranially based skin flap is raised on both sides of the dorsal midline of anesthetized mice. The flap extends the vascular territory of the nourishing lateral thoracic artery and vein (marked in red in *A*). The lateral thoracic artery is ligated. *C*: the flap is sutured back into its original position after interpositioning a silicone sheet to avoid revascularization from the wound bed. *D*: 6 days postoperatively, a clear demarcation can be observed between vital and necrotic flap skin and between healed and nonhealed suture lines.

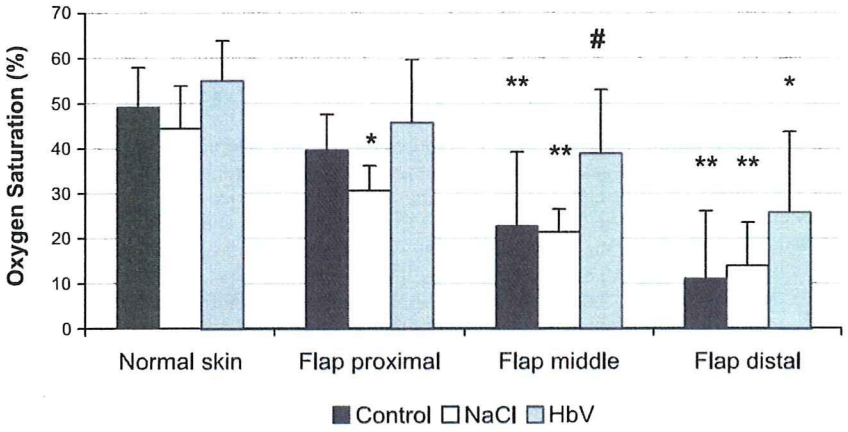

Fig. 2. Oxygen saturation (So_2) in normal skin and proximal, middle, and distal flap skin in untreated control animals and animals receiving 2 × 20% of total blood volume (TBV) of 0.9% NaCl or hemoglobin vesicle (HbV) solution. Data are expressed in mean values and SD. *$P < 0.05$ and **$P < 0.01$ vs. normal skin; #$P < 0.05$ vs. control.

supernatant was collected for measuring HbV-bound Hb and met-Hb concentrations separately.

To assess the pharmacokinetics and plasma viscosity, the plasma of three animals was pooled for each time point. Plasma viscosity was measured with a Höppler-type viscosimeter (HAAKE Messtechnik, Karlsruhe, Germany) at 37°C, and the average of four consecutive measurements was calculated. The plasma concentration of the vesicles was measured with a computerized fluorescence reader (Infinite M 200, Tecan, Maennedorf, Switzerland). For this purpose, the plasma was transferred to 96-well plates. A calibration curve was previously established to transfer fluorescence intensity to vesicle concentration, and native plasma was taken as a negative control.

Protocol. For all manipulations, the animals were anesthetized with intraperitoneal injection of medetomidine (500 μg/kg body wt; Dormitor, Pfizer, Zurich, Switzerland), climazolam (5 mg/kg; Climasol, Gräub, Bern, Switzerland), and fentanyl (50 μg/kg; Fentanyl-Janssen, Janssen-Cilag, Baar, Switzerland), and anesthesia was antagonized by injecting the antidotes atipamezole (1.25 mg/kg body wt; Antisedan, Pfizer), sarmazenil (0.5 mg/kg body wt; Sarmasol, Gräub), and naloxone (0.6 mg/kg; Naloxon, Orpha, Kusnacht, Switzerland) after the manipulations were completed. Animals were euthanized with an overdose of pentobarbital sodium at the end of the experiments.

Immediately after the flap preparation was completed, 20% of the estimated total blood volume of the HbV solution or 0.9% NaCl was injected into the tail vein over a period of 10 min.

On *postoperative day 1*, the cutaneous oxygen saturation measurements were taken, and another 20% of the estimated total blood volume of 0.9% NaCl or the HbV solution was injected.

On *day 6*, tissue survival and primary wound healing were assessed. Thereafter, blood samples were obtained by cardiac puncture for laboratory analysis, and tissue samples were collected for histological examination.

Perioperative death, wound infection, and technical complications such as rupture of the skin suture, thrombosis of the draining vein (leading to total flap loss), or failing arterial ligature (leading to total flap survival) were taken as exclusion criteria.

The same injection protocol was used to determine the pharmacokinetics of the vesicles and the plasma viscosity. Blood samples were obtained by exsanguinating the animals at baseline and 30 min, 24 h, and 48 h after each vesicle solution injection.

Statistical analysis. The InStat version 3.0 software (GraphPad, San Diego, CA) was used for statistical analysis. The data are presented as means ± SD. Differences between the groups or sites of measurements were assessed by unpaired analysis of variance and Bonferroni posttest. A value of $P < 0.05$ was taken to represent statistical significance.

RESULTS

Five animals fulfilled the exclusion criteria (1 death, 1 infection, and 3 technical problems), thus resulting in final sample sizes of $n = 9$ in the control group and $n = 8$ in each other group in the flap experiments.

On *postoperative day 1*, we observed a gradual decrease in oxygen saturation from 49 ± 9% in the normal skin to 11 ± 15% in the distal parts of the flap in all animals (Fig. 2). Whereas similar values were obtained after NaCl injection, higher oxygen saturation was maintained after HbV in all parts of the flap, which became most evident in the middle flap portion ($P < 0.05$).

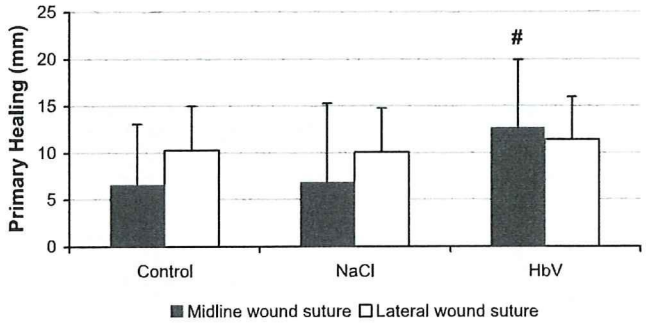

Fig. 3. Length of primarily healed wounds in midline and lateral suture in untreated control animals and animals receiving 2 × 20% of TBV of 0.9% NaCl or HbV solution. Data are expressed in mean values and SD. #$P < 0.05$ vs. control.

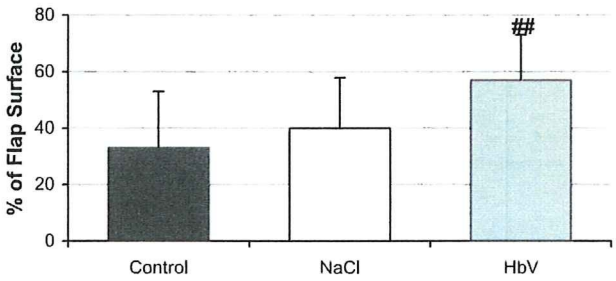

Fig. 4. Flap tissue survival in untreated control animals and animals receiving 2 × 20% of TBV of 0.9% NaCl or HbV solution. Data represent percentages of total flap surface and are expressed in mean values and SD. ##$P < 0.01$ vs. control.

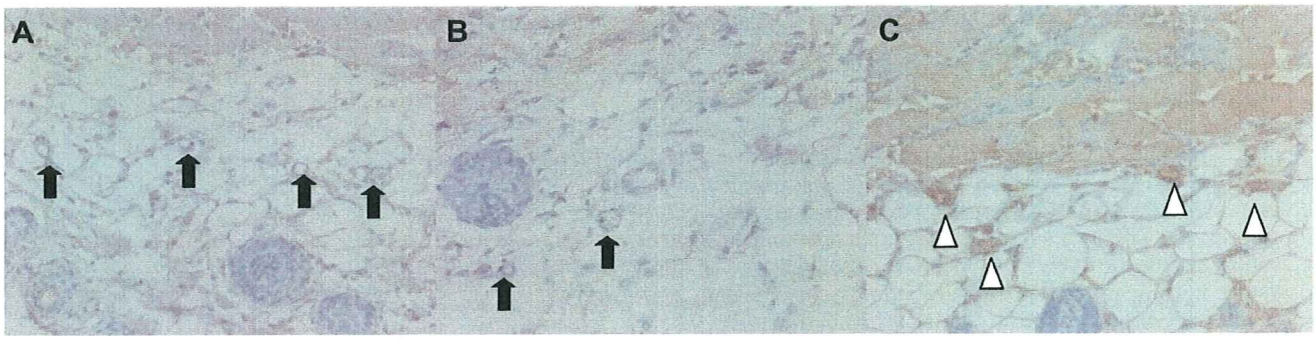

Fig. 5. Immunohistochemical endothelial nitric oxide synthase (eNOS) staining of flap tissue 6 days postoperatively in untreated control animals (*A*) and animals receiving 2 × 20% of TBV of 0.9% NaCl (*B*) or HbV solutions (*C*). Pictures were taken at ×200 magnification. Black arrows exemplary indicate cross-sections of capillaries, whereas white arrowheads indicate capillaries with endothelial cells stained positive for eNOS.

Six days postoperatively, a clear distinction could be made between the healed and nonhealed suture lines, and the demarcation between necrotic and surviving flap tissue was unequivocally discernible (Fig. 1). In the control group, the proximal 6.6 ± 6.5 mm of the midline suture were healed (Fig. 3). This length was increased to 12.7 ± 7.2 mm in the animals having received HbV ($P < 0.05$), whereas it was virtually unchanged in the NaCl group. The mean length of the primarily healed lateral wound ranged between 10.1 and 11.4 mm and was similar in all groups. Flap tissue survival was increased from 33 ± 20% in the control group to 57 ± 16% after HbV ($P < 0.01$) but was similar to control in the NaCl group (Fig. 4).

The immunohistochemical assessment revealed 3.0 ± 0.9 capillaries/visual field in the proximal flap tissue of untreated animals, whereas capillary density was raised to 5.3 ± 0.9 capillaries/visual field after HbV ($P < 0.01$, Figs. 5 and 6). In addition, higher eNOS expression was found in the capillaries of animals treated with the HbV solution, yielding 4.1 ± 1.3 eNOS + capillaries/visual field ($P < 0.01$). The histomorphological examination of the parenchymal tissues exhibited no signs of organ failure, tissue damage (hematoxylin-eosin staining), or leukocyte accumulation (Giemsa staining) in the liver, spleen, and kidney throughout the groups.

Laboratory blood work revealed similar hematocrit levels (means, 41.8% to 44.0%), Hb concentrations (means, 14.1 to 15.0 g/dl), and met-Hb concentrations (means, 0.02% to 0.04%) in all groups 6 days after flap surgery and 5 days after the last injection. No Hb was found in the plasma phase in any animal. The pharmacokinetic experiments revealed that 68% of the initially injected vesicles were still circulating after 24 h. The initial concentrations (88% and 32%) were found 24 and 48 h after the second injection, respectively (Fig. 7). Plasma viscosity was 1.19 cP in the untreated animals, and 1.41 and 1.31 cP at 24 and 48 h after the second vesicle injection, respectively.

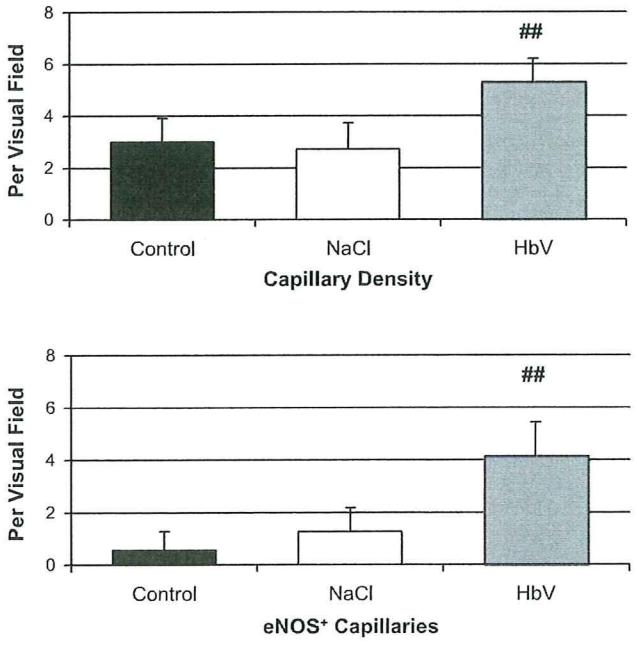

Fig. 6. Capillary density and capillary eNOS expression 6 days postoperatively in untreated control animals and animals receiving 2 × 20% of TBV of 0.9% NaCl or HbV solution. Data are expressed in mean values and SD of capillaries per visual field at ×200 magnification. ##$P < 0.01$ vs. control.

DISCUSSION

The principal findings of the present study were that both the primary healing of the wound between the two ischemic, hypoxic skin margins and the survival of critically ischemic tissue were improved after the administration of left-shifted HbVs.

This biological behavior was paralleled by the pattern of oxygen saturation on the first day after surgery, suggesting that

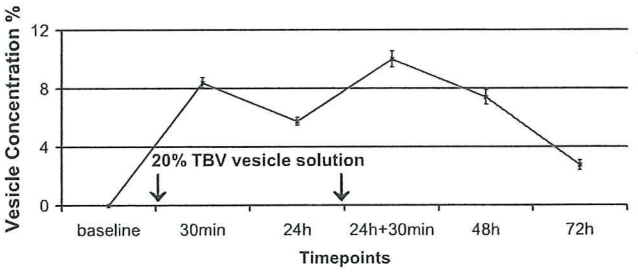

Fig. 7. Vesicle pharmacokinetics. The values represent plasma concentrations of vesicles filled with a sulforhodamin B solution, measured with computerized fluorescence reading before and after receiving 2 × 20% of TBV of vesicle solution. Data are presented in percentages of the concentration present in the injected vesicle solution and are expressed in mean values and SD.

tissue oxygenation was sufficient for survival but not for wound healing in the more proximal parts, whereas the oxygen debt reached a severity that was no longer compatible with cell survival more distally. An increased oxygen demand is necessary for normal tissue repair, which is not sufficiently covered under hypoxic conditions, and wound healing may be attenuated due to the suppression of essential oxygen-dependent processes such as fibroblast and myofibroblast activity, angiogenesis, and collagen synthesis (2, 9). An ameliorated oxygen supply was most likely responsible for the improved midline suture healing in the HbV-treated animals in our study. No such effect was observed in the lateral wound margins where tissue repair appeared to be in the domain of the healthy, normoxic skin, not affected by the HbVs. The length of the lateral, primarily healed suture line corresponded to the length of the healed midline suture line in the animals receiving HbV, thus emphasizing the therapeutic potential of this oxygen carrier.

The immunohistochemical analysis yielded significantly higher capillary counts and eNOS expression in the flap tissue of animals receiving HbVs. eNOS exerts a predominant function in angiogenesis and vasculogenesis (7). Besides stimulating new vessel formation, it attenuates endothelial cell apoptosis (1, 15). eNOS is therefore a pivotal player in wound healing (3, 14) and contributes to maintain or improve flap tissue survival (11, 13). eNOS expression is oxygen dependent (12, 16, 23), stimulated by fluid shear stress (15, 24), and inhibited by proinflammatory cytokines (1, 23, 27).

Each of these pathways may have been influenced by the HbVs. With the assumption that the NaCl and H_2O components of the administered solutions exited the vascular compartment within a few minutes, the administered dosage of HbVs enhanced the HbV concentration in the whole blood by ~15% after the first injection, and according to the pharmacokinetic experiments, one third of the initially injected amount of HbVs was still circulating 3 days later. Much more importantly than increasing the oxygen carrying capacity, the HbVs regulate oxygen release from the red blood cells to the tissue due to their presence in the plasma phase. If the oxygen affinity of the HbV is increased, a higher oxygen tension gradient is required for oxygen release to the tissue. Thus oxygen release is shifted to the downstream vasculature (26), redistributing oxygen in favor of ischemic, hypoxic tissues (25). The advantage of left-shifting HbV oxygen affinity for this purpose was repeatedly demonstrated in our previous works (5, 6). Furthermore, the HbVs increased plasma viscosity, which has been made responsible for improved microcirculatory blood flow (5, 6, 8, 17, 18), both enhancing shear stress on the vascular lining. In our previous studies, a beneficial effect of the left-shifted HbVs on ischemic flap tissue has been shown for several secondary end points including tissue energy metabolism (5), apoptosis (17), proinflammatory cytokines, and leukocyte activation (18).

To weigh the biological performance of the biomaterial against its possible adverse effects, we performed pathohistomorphological examinations in the organs at risk, which is where HbVs are degraded and excreted, such as in the liver, spleen, and kidney (20). Although our test animals received large amounts of HbV, it was completely metabolized after six days, and no tissue alterations or damages were seen at this time point. These findings are in line with extended histomorphological and laboratory investigations performed by Sakai et al. (21, 22) in rats.

From our results, we conclude that left-shifted HbVs may ameliorate the survival and primary healing of critically ischemic wound margins, possibly by stimulating eNOS-mediated neovascularization.

GRANTS

This research was supported by Swiss National Foundation for Scientific Research Grants 32-065149.01 and 32-108408.05; by the Department of Clinical Research, University of Berne, Switzerland; by a Health and Labour Sciences Research grant from the Ministry of Health, Labour and Welfare, Japan; and by from the Japan Society for the Promotion of Science Grant-in-Aid for Scientific Research B19300164.

REFERENCES

1. **Agnoletti L, Curello S, Bachetti T, Malacarne F, Gaia G, Comini L, Volterrani M, Bonetti P, Parrinello G, Cadei M, Grigolato PG, Ferrari R.** Serum from patients with severe heart failure downregulates eNOS and is proapoptotic: role of tumor necrosis factor-alpha. *Circulation* 100: 1983–1991, 1999.
2. **Alizadeh N, Pepper MS, Modarressi A, Alfo K, Schlaudraff K, Montandon D, Gabbiani G, Bochaton-Piallat ML, Pittet B.** Persistent ischemia impairs myofibroblast development in wound granulation tissue: a new model of delayed wound healing. *Wound Repair Regen* 15: 809–816, 2007.
3. **Breen AM, Dockery P, O'Brien T, Pandit AS.** The use of therapeutic gene eNOS delivered via a fibrin scaffold enhances wound healing in a compromised wound model. *Biomaterials* 29: 3143–3151, 2008.
4. **Chang TM.** Artificial cells for cell and organ replacements. *Artif Organs* 28: 265–270, 2004.
5. **Contaldo C, Plock J, Sakai H, Takeoka S, Tsuchida E, Leunig M, Banic A, Erni D.** New generation of hemoglobin-based oxygen carriers evaluated for oxygenation of critically ischemic hamster flap tissue. *Crit Care Med* 33: 806–812, 2005.
6. **Contaldo C, Schramm S, Wettstein R, Sakai H, Takeoka S, Tsuchida E, Leunig M, Banic A, Erni D.** Improved oxygenation in ischemic hamster flap tissue is correlated with increasing hemodilution with Hb vesicles and their O_2 affinity. *Am J Physiol Heart Circ Physiol* 285: H1140–H1147, 2003.
7. **Duda DG, Fukumura D, Jain RK.** Role of eNOS in neovascularization: NO for endothelial progenitor cells. *Trends Mol Med* 10: 143–145, 2004.
8. **Erni D, Wettstein R, Schramm S, Contaldo C, Sakai H, Takeoka S, Tsuchida E, Leunig M, Banic A.** Normovolemic hemodilution with Hb vesicle solution attenuates hypoxia in ischemic hamster flap tissue. *Am J Physiol Heart Circ Physiol* 284: H1702–H1709, 2003.
9. **Gordillo GM, Sen CK.** Revisiting the essential role of oxygen in wound healing. *Am J Surg* 186: 259–263, 2003.
10. **Gottrup F.** Oxygen in wound healing and infection. *World J Surg* 28: 312–315, 2004.
11. **Huang N, Khan A, Ashrafpour H, Neligan PC, Forrest CR, Kontos CD, Pang CY.** Efficacy and mechanism of adenovirus-mediated VEGF-165 gene therapy for augmentation of skin flap viability. *Am J Physiol Heart Circ Physiol* 291: H127–H137, 2006.
12. **Jelic S, Padeletti M, Kawut SM, Higgins C, Canfield SM, Onat D, Colombo PC, Basner RC, Factor P, LeJemtel TH.** Inflammation, oxidative stress, and repair capacity of the vascular endothelium in obstructive sleep apnea. *Circulation* 117: 2270–2278, 2008.
13. **Kuo YR, Wang FS, Jeng SF, Lutz BS, Huang HC, Yang KD.** Nitrosoglutathione promotes flap survival via suppression of reperfusion injury-induced superoxide and inducible nitric oxide synthase induction. *J Trauma* 57: 1025–1031, 2004.
14. **Lee PC, Salyapongse AN, Bragdon GA, Shears LL 2nd, Watkins SC, Edington HD, Billiar TR.** Impaired wound healing and angiogenesis in eNOS-deficient mice. *Am J Physiol Heart Circ Physiol* 277: H1600–H1608, 1999.
15. **Metaxa E, Meng H, Kaluvala SR, Szymanski MP, Paluch RA, Kolega J.** Nitric oxide-dependent stimulation of endothelial cell proliferation by sustained high flow. *Am J Physiol Heart Circ Physiol* 295: H736–H742, 2008.
16. **Ostergaard L, Stankevicius E, Andersen MR, Eskildsen-Helmond Y, Ledet T, Mulvany MJ, Simonsen U.** Diminished NO release in chronic

hypoxic human endothelial cells. *Am J Physiol Heart Circ Physiol* 293: H2894–H2903, 2007.

17. **Plock J, Contaldo C, Sakai H, Tsuchida E, Leunig M, Banic A, Menger M, Erni D.** Is hemoglobin in hemoglobin vesicles infused for isovolemic hemodilution necessary to improve oxygenation in critically ischemic hamster skin? *Am J Physiol Heart Circ Physiol* 289: H2624–H2631, 2005.
18. **Plock J, Tromp A, Contaldo C, Spanholtz T, Sinovcic D, Sakai H, Tsuchida E, Leunig M, Banic A, Erni D.** Hemoglobin vesicles reduce hypoxia-related inflammation in critically ischemic hamster flap tissue. *Crit Care Med* 35: 899–905, 2007.
19. **Sakai H, Hara H, Yuasa M, Tsai A, Takeoka S, Tsuchida E, Intaglietta M.** Molecular dimensions of Hb-based O_2 carriers determine constriction of resistance arteries and hypertension. *Am J Physiol Heart Circ Physiol* 279: H908–H915, 2000.
20. **Sakai H, Horinouchi H, Masada Y, Takeoka S, Ikeda E, Takaori M, Kobayashi K, Tsuchida E.** Metabolism of hemoglobin-vesicles (artificial oxygen carriers) and their influence on organ functions in a rat model. *Biomaterials* 25: 4317–4325, 2004.
21. **Sakai H, Horinouchi H, Tomiyama K, Ikeda E, Takeoka S, Kobayashi K, Tsuchida E.** Hemoglobin-vesicles as oxygen carriers: influence on phagocytic activity and histopathological changes in reticuloendothelial system. *Am J Pathol* 159: 1079–1088, 2001.
22. **Sakai H, Masada Y, Horinouchi H, Ikeda E, Sou K, Takeoka S, Suematsu M, Takaori M, Kobayashi K, Tsuchida E.** Physiological capacity of the reticuloendothelial system for the degradation of hemoglobin vesicles (artificial oxygen carriers) after massive intravenous doses by daily repeated infusions for 14 days. *J Pharmacol Exp Ther* 311: 874–884, 2004.
23. **Searles CD.** Transcriptional and posttranscriptional regulation of endothelial nitric oxide synthase expression. *Am J Physiol Cell Physiol* 291: C803–C816, 2006.
24. **Tao J, Yang Z, Wang JM, Tu C, Pan SR.** Effects of fluid shear stress on eNOS mRNA expression and NO production in human endothelial progenitor cells. *Cardiology* 106: 82–88, 2006.
25. **Tsai A, Vandegriff K, Intaglietta M, Winslow R.** Targeted O_2 delivery by low-P_{50} hemoglobin: a new basis for O_2 therapeutics. *Am J Physiol Heart Circ Physiol* 285: H1411–H1419, 2003.
26. **Vadapalli A, Goldman D, Popel A.** Calculations of oxygen transport by red blood cells and hemoglobin solutions in capillaries. *Artif Cells Blood Substit Immobil Biotechnol* 30: 157–188, 2002.
27. **Yan G, You B, Chen SP, Liao JK, Sun J.** Tumor necrosis factor-alpha downregulates endothelial nitric oxide synthase mRNA stability via translation elongation factor 1-alpha 1. *Circ Res* 103: 591–597, 2008.

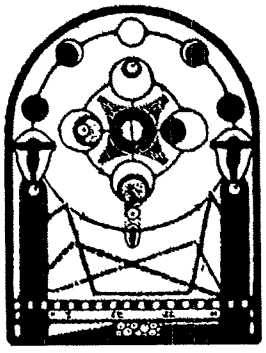

The role of an amino acid triad at the entrance of the heme pocket in human serum albumin for O_2 and CO binding to iron protoporphyrin IX†

Teruyuki Komatsu,*[a,b] Akito Nakagawa,[a] Stephen Curry,[c] Eishun Tsuchida,[a] Kenichi Murata,[d] Nobuhumi Nakamura[d] and Hiroyuki Ohno[d]

Received 19th May 2009, Accepted 29th June 2009
First published as an Advance Article on the web 22nd July 2009
DOI: 10.1039/b909794e

Complexation of iron(II) protoporphyrin IX (Fe^{2+}PP) into a genetically engineered heme pocket on recombinant human serum albumin (rHSA) creates an artificial hemoprotein which can bind O_2 reversibly at room temperature. Here we highlight a crucial role of a basic amino acid triad the entrance of the heme pocket in rHSA (Arg-114, His-146, Lys-190) for O_2 and CO binding to the prosthetic Fe^{2+}PP group. Replacing His-146 and/or Lys-190 with Arg resolved the structured heterogeneity of the possible two complexing modes of the porphyrin and afforded a single O_2 and CO binding affinity. Resonance Raman spectra show only one geometry of the axial His coordination to the central ferrous ion of the Fe^{2+}PP.

Introduction

Hemin [iron(III) protoporphyrin IX (Fe^{3+}PP), Fig. 1] dissociated from methemoglobin (metHb) is potentially toxic in the human body, because it intercalates in phospholipid membranes and participates in Fenton's reaction to produce hydroxyl radicals.[1] Hemopexin (Hpx, 60,000 Da), a β-glycoprotein in plasma (< 17 μM), captures the Fe^{3+}PP with an extraordinarily high binding affinity ($K > 10^{12}$ M^{-1}) and transports it to the liver for catabolism.[2] When Hpx becomes saturated (*e.g.* as a result of serious hemolytic injuries), the Fe^{3+}PP is first bound by human serum albumin (HSA, 66,500 Da) ($K = 1.1 \times 10^8$ M^{-1}),[3,4] the most abundant plasma protein (*ca.* 650 μM), and then transferred to Hpx. The biological function of the HSA–Fe^{3+}PP complex has attracted considerable interest for many years. However, Casella *et al.* reported little peroxidase or catalase activity,[5] so this naturally occurring hemoprotein may not play any significant role in vivo. If anything, HSA may serve to keep the incorporated hemin group physiologically silent.

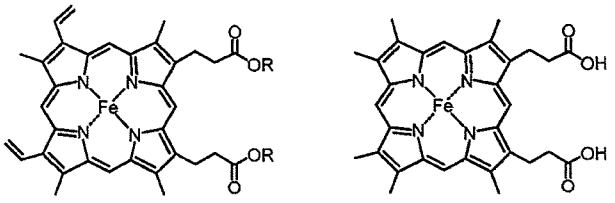

Fig. 1 Chemical formula of Fe porphyrins.

Crystal structure analysis of HSA–Fe^{3+}PP revealed that Fe^{3+}PP is bound within a deep hydrophobic slot in subdomain IB of HSA with axial coordination to the side-chain hydroxyl of Tyr-161 and salt bridges between the porphyrin propionates and a triad of basic amino acid residues at the pocket entrance (Arg-114, His-146, and Lys-190) (Fig. 2).[6,7] While the reduced ferrous HSA–Fe^{2+}PP is immediately autoxidized by O_2,[5] we found that a pair of site-specific mutations into the subdomain IB of HSA allows the Fe^{2+}PP to bind O_2: introduction of a proximal His at the Leu-185 position and substitution of the coordinated Tyr-161 with non-polar Leu (Y161L/L185H [rHSA**1**]) (Fig. 2).[9b,d] Remarkably, introduction of the proximal His at the Ile-142 position (on the opposite side of the porphyrin ring plane) also confers O_2 binding capability to the Fe^{2+}PP (I142H/Y161L [rHSA**2**]).[9a,c,d] These albumin O_2 transporters may serve as an effective red blood cell (RBC) substitute if the O_2 binding affinity is sufficient for clinical use. However, rHSA**1**–Fe^{2+}PP and rHSA**2**–Fe^{2+}PP both show two O_2 binding affinities ($P_{1/2}{}^{O2}$). The major component (species I, 60–75%) exhibits similar $P_{1/2}{}^{O2}$ to that of human RBC ($P_{1/2}{}^{O2} = 8$ Torr), but the minor component (species II, 25–40%) shows only a seventh to a tenth of the affinity (Table 1).[9] Our explanation for this observation is that the porphyrin plane of Fe^{2+}PP binds in the pocket in either of two alternative orientations (180° rotational isomers) that have slightly different geometries of axial His coordination to the central ferrous ion, only one of which confers high affinity O_2 binding.[9] Since less than 20% of species II of rHSA**2**–Fe^{2+}PP ($P_{1/2}{}^{O2} = 134$ Torr) is dioxygenated in the human lung's conditions ($P_{O2} = ca.$ 110 Torr, 37 °C), the low O_2 binding affinity component cannot effectively deliver O_2 to the tissues and should be excluded to develop this promising O_2 carrying plasma protein as an RBC substitute. Interestingly, a similar dependence of O_2 binding affinities on the orientations of the porphyrin ring

[a]*Research Institute for Science and Engineering, Waseda University, 3-4-1 Okubo, Shinjuku-ku, Tokyo, 169-8555, Japan. E-mail: teruyuki@waseda.jp; Fax: (+81) 3 5286 3148*
[b]*PRESTO, Japan Science and Technology Agency (JST), Japan. 4-1-8 Honcho, Kawaguchi-shi, Saitama, 332-0012, Japan*
[c]*Biophysics Section, Blackett Laboratory, Imperial College London, Exhibition Road, London, SW7 2AZ, United Kingdom*
[d]*Department of Biotechnology and Life Science, Tokyo University of Agriculture and Technology, 2-24-16, Naka-cho, Koganei-shi, Tokyo 184-8588, Japan*

† Electronic supplementary information (ESI) available: UV-vis absorption spectral data of rHSA–FePP and rHSA–FeDMDP, and absorption decay of CO rebinding to rHSA**2**–Fe^{2+}DMDP after laser flash photolysis. See DOI: 10.1039/b909794e

Table 1 O_2 and CO binding parameters of rHSA–Fe^{2+}PP in 50 mM potassium phosphate buffered solution (pH 7.0) at 22 °C

	k_{on}^{O2} ($\mu M^{-1}s^{-1}$)	k_{off}^{O2} (ms^{-1})		$P_{1/2}^{O2}$ (Torr)		k_{on}^{CO} ($\mu M^{-1}s^{-1}$)		k_{off}^{CO} (s^{-1})		$P_{1/2}^{CO}$ (Torr)	
		I	II	I	II	I	II	I	II	I	II
rHSA**1**–Fe^{2+}PP[a]	31	0.20	2.1	4	41	3.7	0.35	0.012	0.077	0.0026	0.18
rHSA**2**–Fe^{2+}PP[a]	7.5	0.22	1.7	18	134	2.0	0.27	0.013	0.079	0.0053	0.24
rHSA**1**(H146R)–Fe^{2+}PP	43	0.37	—	6	—	5.1	—	0.013	—	0.0033	—
rHSA**1**(L190R)–Fe^{2+}PP	24	0.35	—	9	—	4.0	—	0.010	—	0.0031	—
rHSA**1**(H146R/K190R)–Fe^{2+}PP	42	0.41	—	6	—	6.1	—	0.011	—	0.0022	—
rHSA**2**(H146R/K190R)–Fe^{2+}PP	11	0.30	—	17	—	1.7	—	0.012	—	0.0058	
Mb[b]	14	0.012		0.51		0.51		0.019		0.030	

[a] Ref. 9b. [b] Sperm whale Mb in 0.1 M potassium phosphate buffer (pH 7.0, 20 °C); ref. 17.

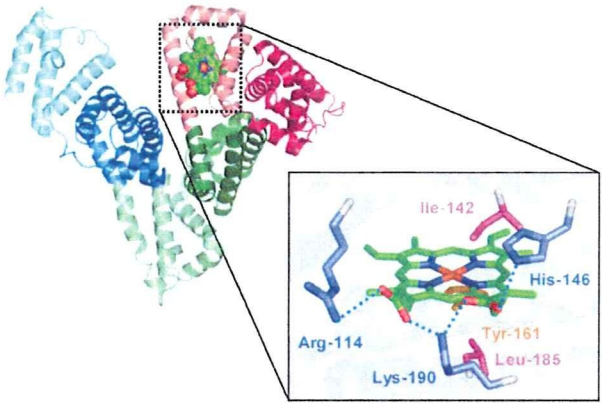

rHSA	Position				
	142	146	161	185	190
Wild type (WT)	Ile	His	Tyr	Leu	Lys
1	Ile	His	Leu	His	Lys
2	His	His	Leu	Leu	Lys
1(H146R)	Ile	Arg	Leu	His	Lys
1(K190R)	Ile	His	Leu	His	Arg
1(H146R/K190R)	Ile	Arg	Leu	His	Arg
2(H146R/K190R)	His	Arg	Leu	Leu	Arg

Fig. 2 Structure of the heme pocket in the rHSA(WT)–hemin complex (PDB ID: 1O9X from ref. 7).[8] Positions of the amino acids where site-specific mutations were introduced and abbreviations of the mutants are shown in the table.

plane is found in insect Hb.[10] If one could prepare a desired heme pocket architecture to distinguish the two possible binding modes of the asymmetric Fe^{2+}PP, it would provide new insights into the modulation of hemoprotein chemistry.

In this paper we report for the first time a role for the basic amino acid triad at the entrance of the heme pocket in rHSA in regulating O_2 and CO binding to the prosthetic Fe^{2+}PP group. Replacing His-146 and/or Lys-190 with Arg in rHSA**1**–Fe^{2+}PP and rHSA**2**–Fe^{2+}PP resolved the structural heterogeneity of the porphyrin plane orientation and afforded a single high-affinity O_2 and CO binding equilibrium. Moreover, the O_2 binding affinities of these hemoproteins are all similar to that of RBC. Resonance Raman (RR) spectra clearly show one geometry of the axial His coordination to Fe^{2+}PP.

Results and discussion

Design of the heme pocket

To bind the hemin molecule tightly, HSA exploits multiple electrostatic interactions between three basic amino acid residues and the hemin propionates at the wide entrance of the heme pocket (Fig. 2). Lys-190 adopts a central position and makes salt bridges to both propionic acid side chains. His-146 and Arg-114 provide a second electrostatic coordination with each carboxylate. Notably, the UV-vis absorption spectrum of HSA complexed with an iron(III) protoporphyrin IX dimethylester (Fe^{3+}PPDM, Fig. 1) showed very broad Soret and Q bands, suggesting that Fe^{3+}PPDM without peripheral carboxylic acids may not be bound stably within subdomain IB. This suggested that modification of this key basic amino acid triad involved in coordinating the hemin propionates could be used to regulate the orientation of the porphyrin ring plane in subdomain IB. We designed four new rHSA mutants based on the existing pair of double mutants that contain the substitutions necessary to confer O_2 binding to the Fe^{2+}PP (Y161L/L185H or I142H/Y161L).[9] His-146 and Lys-190 were replaced by more bulky and basic Arg: H146R, K190R, and H146R/K190R mutations were combined with the O_2 binding mutations (see Fig. 2 for details). We postulated that the introduction of Arg residues would reduce the space available at the entrance to the cavity and might thereby restrict the binding of Fe^{2+}PP to a single conformation.

Site-specific mutations were introduced into the HSA coding region in a plasmid vector (pHIL-D2 HSA). The proteins were expressed in the yeast species *Pichia pastoris*. The rHSA–Fe^{2+}PP complexes were prepared according to our previously reported procedures (see Experimental).

O_2 and CO binding properties of rHSA–Fe^{2+}PP

The UV-vis absorption spectra of all six rHSA(mutant)–Fe^{3+}PP were essentially identical (Fig. 3, Table S1†). They were easily reduced to the corresponding ferrous complexes by adding a small amount of degassed aqueous $Na_2S_2O_4$ under an N_2 atmosphere. A single broad absorption band (λ = 558–559 nm) in the visible region signified the formation of a five-*N*-coordinate high-spin complex similar to deoxy Mb[11] or the synthetic chelated heme in DMF.[12] The spectral features and amplitude did not change in the temperature range of 5–25 °C. These observations show that the guanidinium groups of Arg-146 or Arg-190 do *not* interact with

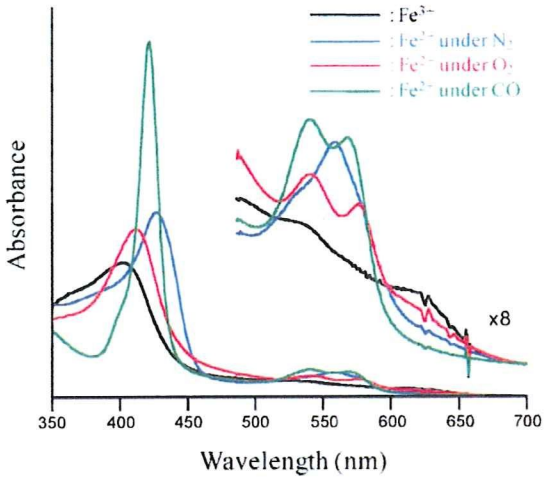

Fig. 3 UV-vis absorption spectral changes of rHSA**1**(H146R/K190R)–Fe^{2+}PP in 50 mM potassium phosphate buffered solution (pH 7.0) at 22 °C.

the ferrous iron of the Fe^{2+}PP, since the resulting formation of a six-*N*-coordinate low-spin complex would have yielded sharp and split α, β bands in the visible region[9c] and been sensitive to rapid oxidation by O_2 *via* an outer sphere mechanism.[13]

Upon exposure of the rHSA–Fe^{2+}PP solution to O_2 gas, the UV-vis absorption changed to that of the dioxygenated complex (Fig. 3).[9,11] After exposure to flowing CO, the Fe^{2+}PP produced a typical carbonyl complex.

We then used laser flash photolysis spectroscopy to determine association and dissociation rate constants (k_{on}, k_{off}) for O_2 and CO binding to rHSA–Fe^{2+}PP.[9] The time dependence of the absorption change accompanying the CO recombination to rHSA**1**–Fe^{2+}PP and rHSA**2**–Fe^{2+}PP obeyed double-exponentials, although the O_2 binding kinetics followed a single-exponential.[9] The slow phase (species II) of the CO rebinding showed 7–11-fold lower k_{on}^{CO} and 6-fold higher k_{off}^{CO} than those of the fast phase (species I) (Table 1). We interpreted this to mean that the low O_2 binding affinity conformers of rHSA**1**–Fe^{2+}PP and rHSA**2**–Fe^{2+}PP have bending strain in the proximal His coordination.[9,14–16] In contrast, the rebinding kinetics of O_2 and CO to rHSA**1**(H146R)–Fe^{2+}PP, rHSA**1**(K190R)–Fe^{2+}PP, rHSA**1**(H146R/K190R)–Fe^{2+}PP and rHSA**2**(H146R/K190R)–Fe^{2+}PP were strictly monophasic (Fig. 4). As a result, these hemoproteins showed single O_2 and CO binding affinity ($P_{1/2}^{O2}$ and $P_{1/2}^{CO}$), which were all similar to the higher affinities (species I) of the original double mutants (Table 1). We can conclude that the introduction of Arg into the entrance of the heme pocket of rHSA**1** and rHSA**2** is effective at excluding the low O_2 binding affinity conformer.

CO binding to rHSA–Fe^{2+}DMDP

To verify our interpretation that the replacement of H146 and/or K190 by Arg resolved the structural heterogeneity of the two complexing modes of the Fe^{2+}PP and gave a single O_2 and CO binding affinity, we examined the incorporation of a symmetrical iron(II) 2,4-dimethyl-deuteroporphyrin (Fe^{2+}DMDP, Fig. 1) as an active site. The UV-vis absorption spectrum of

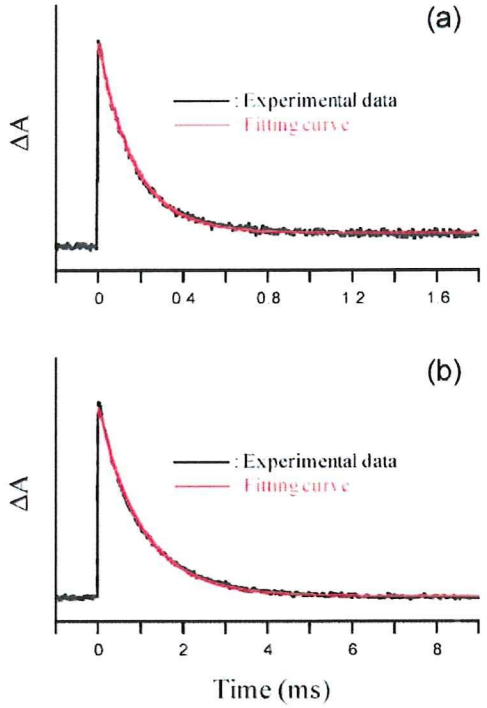

Fig. 4 Absorption decay of O_2 and CO rebinding to rHSA**1**(H146R/K190R)–Fe^{2+}PP after the laser flash photolysis at 22 °C; (a) O_2 and (b) CO. Both kinetics were composed of monophasic phases. A relaxation curve was fitted single exponential (red line).

the ferric rHSA**2**–Fe^{3+}DMDP showed a very similar pattern to that of rHSA**2**–Fe^{3+}PP though each λ_{max} value was hypsochromic (8–11 nm) shifted (Table S1†). The reduced ferrous form of rHSA**2**–Fe^{2+}DMDP under an N_2 atmosphere exhibited a slightly broadened Soret band absorption, but the main species was a five-*N*-coordinate high spin complex involving axial His-142 coordination. Upon introduction of O_2 gas through the solution, rHSA**2**–Fe^{2+}DMDP bound O_2 only at 5 °C and was observed to autoxidize at 22 °C. In general, the stability of the O_2 adduct complex of a heme derivative is sensitive to the electron density at Fe^{2+} and thus to the substituents at the porphyrin periphery.[18,19] Our attempt to determine the O_2 binding parameters of rHSA**2**–Fe^{2+}DMDP unfortunately failed. However, after introduction of CO gas, rHSA**2**–Fe^{2+}DMDP produced a stable carbonyl complex. We again used laser flash photolysis to characterize the CO binding properties of this hemoprotein. As expected, the absorption decay associated with CO recombination with rHSA**2**–Fe^{2+}DMDP was clearly monophasic (Fig. S1†). This result implied that the symmetric Fe^{2+}DMDP molecule is accommodated in subdomain IB of rHSA**2** in a single orientation and there is only one geometry of the axial His-142 coordination to the central ferrous ion of Fe^{2+}DMDP. Interestingly, the CO rebinding to rHSA**2**–Fe^{2+}DMDP (k_{on}^{CO}: 0.42 $\mu M^{-1}s^{-1}$) was relatively slow compared to that of rHSA**2**–Fe^{2+}PP and similar to Mb.[17]

RR and IR spectroscopies

The RR and infrared (IR) spectra of these artificial hemoproteins also supported the results described above. The stretching